KUOPION YLIOPISTON JULKAISUJA G. - A.I. VIRTANEN -INSTITUUTTI 75
KUOPIO UNIVERSITY PUBLICATIONS G.
A.I. VIRTANEN INSTITUTE FOR MOLECULAR SCIENCES 75

KIMMO JOKIVARSI

Probing Water Dynamics in Acute Cerebral Ischemia by MRI

Doctoral dissertation

To be presented by permission of the Faculty of Natural and Environmental Sciences
of the University of Kuopio for public examination
in TTA Auditorium, Tietoteknia building, University of Kuopio,
on Monday 21st September 2009, at 1 p.m.

Department of Neurobiology
A.I. Virtanen Institute for Molecular Sciences
University of Kuopio

KUOPION YLIOPISTO
KUOPIO 2009

Distributor: Kuopio University Library
P.O. Box 1627
FI-70211 KUOPIO
FINLAND
Tel. +358 40 355 3430
Fax +358 17 163 410
http://www.uku.fi/kirjasto/julkaisutoiminta/julkmyyn.shtml

Series Editors: Professor Olli Gröhn, Ph.D.
Department of Neurobiology
A.I. Virtanen Institute for Molecular Sciences

Professor Michael Courtney, Ph.D.
Department of Neurobiology
A.I. Virtanen Institute for Molecular Sciences

Author's address: Department of Neurobiology
A.I. Virtanen Institute for Molecular Sciences
University of Kuopio
P.O. Box 1627
FI-70211 KUOPIO
FINLAND
Tel. +358 40 355 2012
Fax +358 17 163 030
E-mail: Kimmo.Jokivarsi@uku.fi

Supervisors: Professor Risto A. Kauppinen, M.D., Ph.D.
Biomedical NMR Research Center
Dartmouth Medical School
Hanover, NH, USA

Professor Olli Gröhn, Ph.D.
Department of Neurobiology
A.I. Virtanen Institute for Molecular Sciences
University of Kuopio

Reviewers: Professor Turgut Tatlisumak, M.D., Ph.D.
Department of Neurology
Helsinki University Central Hospital

Assistant Professor Phillip Zhe Sun, Ph.D.
Department of Radiology
Harvard Medical School
Boston, USA

Opponent: Professor Steven C.R. Williams, Ph.D.
Institute of Psychiatry
King's College
London, UK

ISBN 978-951-27-1134-5
ISBN 978-951-27-1115-4 (PDF)
ISSN 1458-7335

Kopijyvä
Kuopio 2009
Finland

Jokivarsi, Kimmo. Probing Water Dynamics in Acute Ischemic Stroke by MRI. Kuopio University Publications G. -A.I. Virtanen Institute for Molecular Sciences 75. 2009. 77 p.
ISBN 978-951-27-1134-5
ISBN 978-951-27-1115-4 (PDF)
ISSN 1458-7335

ABSTRACT

Cerebral ischemia that leads to stroke is one of the major causes of disability and death in Finland and around the world. After sustaining ischemic damage due to lack of oxygen and glucose, cerebral tissue undergoes a complex time-dependent cascade of heterogeneous histopathological changes. Following an ischemic attack, patients require fast and accurate diagnostic tools to characterize their cerebral tissue state upon hospital admission. New treatment methods for stroke are being discovered and are under investigation. Therefore, to select the most appropriate treatment method for each patient a thorough overview of the ischemic tissue status is needed. Furthermore, in experimental studies a way to accurately predict tissue damage without intervention gives an opportunity to study and compare new treatment modalities.

Magnetic resonance imaging (MRI) is a sensitive method to assess local changes in tissue water during ischemia. Several different MRI contrasts can be exploited to assess blood flow and perfusion, diffusion of water and changes in the water molecule environment. These biophysical and pathological changes give information about the state and progression of ischemic damage in tissue. However, each of these MRI contrasts only tells about one aspect of the complex dynamic changes that are happening during ischemia. Multiple MRI techniques in combination must be applied to attain a better overview of the status of the brain tissue. Furthermore, a significant difference in measured lesion sizes can be seen when using diffusion and perfusion MRI during early stages of acute ischemia. This highlights the difference of the contrasts as they have very different and specific temporal evolution. This discrepancy in the projected lesion size is considered the area of transition from viable to irreparably damaged tissue; an area, where changes are happening, but that can be reversed or stopped with a timely intervention. This is an important target to recognize for treatment planning to maximize the benefit and minimize the side effects of a therapeutic intervention.

The aim of this study was to study acute brain ischemia in rats with advanced MRI techniques with a view to increase the understanding of changes in tissue water. We investigated the dynamic changes in MRI parameters in ischemic brain during hyperacute ischemia. Apart from the established MRI contrasts - diffusion, perfusion and T_2 and T_1 relaxation times - also more novel contrasts were utilized, such as rotating frame contrasts $T_{1\rho}$ and $T_{2\rho}$ and amide proton transfer ratio (APTR) contrasts. The rotating frame contrast techniques probe the molecular motion and the different molecular environments during stroke. APTR is connected with pH and can be used to image the changes in the acidity relating to the energy state of the tissue. The MRI parameters were measured at multiple time points to assess the temporal evolution of ischemia. This multiparametric MRI approach provided complementary information from different aspects of the ischemic pathway.

Partially due to the high socio-economical impact of stroke there is active research both to prevent conditions that lead to an increased risk of stroke and to find new treatment methods to prevent further injury during ischemia. This also creates incentive to investigate more accurate methods to assess the state of stroke and the effectiveness of novel pharmaceuticals. This work demonstrated that multiparametric MRI has the potential to accurately assess and predict ischemic damage. With optimization of the imaging protocols MRI can be an indispensable tool both in pre-clinical and clinical stroke imaging.

National Library of Medicine Classification: WL 355, WL 302, WN 185
Medical Subject Headings: Cerebrovascular Disorders/diagnosis; Stroke/diagnosis; Brain Ischemia/diagnosis; Cerebral Infarction/diagnosis; Cerebral Hemorrhage/diagnosis; Diagnostic Imaging; Magnetic Resonance Imaging; Magnetic Resonance Spectroscopy; Blood Circulation; Cerebrovascular Circulation; Hypoxia, Brain/diagnosis; Water; Lactic Acid; Hydrogen-Ion Concentration; Disease Models, Animal; Rose Bengal; Rats

After spending hundreds of hours working with a pile of data
ending up with only one or two small pictures
and disregarding 95% of the analysis.
It gives a perspective
to the old saying:
It is the journey
not the goal.

ACKNOWLEDGEMENTS

These studies were carried out at the A. I. Virtanen Institute for Molecular Sciences, University of Kuopio, during the years 2004-2009.

I want to sincerely thank my principal supervisor Professor Risto Kauppinen and my principal local supervisor in Kuopio, Professor Olli Gröhn, for giving me this hands-on chance to learn a new modality in medical imaging and for all the invaluable guidance along the way in the world of biomedical magnetic resonance imaging.

I want to thank the official reviewers of this thesis, Professors Turgut Tatlisumak and Phillip Zhe Sun for their efforts, comments and constructive criticism.

I also want to thank my co-authors, especially Doctor Heidi Gröhn for setting the groundwork for my thesis, Professor Yrjö Hiltunen for fruitful discussions about data modeling, Docent Jukka Jolkkonen, Doctors Shalom Michaeli, Michael Garwood, Teemu Laitinen, Pasi Tuunanen and Mr Juha-Pekka Niskanen for their invaluable input for the articles and Mr Nick Hayward for proofreading the manuscripts and this thesis.

I am very grateful to Ms Maarit Pulkkinen for her great work with the animals and for her continuous efforts in organizing things in the lab to make things run smoothly, Ms Tiina Konu for preparing some of the animals for MRI and Doctor Alejandra Sierra-Lopez and Mr Xavier Ekolle Ndode-Ekane for showing me how to do histological imaging and cell counting.

I want to thank all my colleagues: Antti Airaksinen, Jaak Nairismägi, Joanna Huttunen, Johanna Närväinen, Juha-Pekka Niskanen, Kimmo Lehtimäki, Lauri Lehto, Martin Kavec, Nick Hayward, Otto Manninen, Pasi Tuunanen, Piia Valonen, Alejandra Sierra-Lopez, Teemu Laitinen and Timo Liimatainen for their much appreciated help along the way. I have had several nice moments of conversation with many of you, whether it was about chili peppers, computers, weather, and world in general … - or MRI.

I want to warmly thank the personnel at the A. I. Virtanen Institute, especially Kaija Pekkarinen, Heidi Levinheimo, Leena Lampinen, Riitta Laitinen and Riitta Keinänen for clearing up the official paperwork knots and Pekka Ala-Kuijala, Jouko Mäkäräinen and Jari Nissinen for random technical assistance.

I also want to thank all the people at the A. I. Virtanen Institute that I have met along the way, who have filled these years with new ideas, perspectives and experiences.

Furthermore, I want to say a warm thank you to Professors Alfred R. Smith, Thomas Bortfeld and Anna-Liisa Brownell who gently persuaded me to do a PhD that I did manage to postpone for several years.

Finally, I want to thank my parents for their love and continual support in letting me follow my path.

And a very special thank you to Piia for her love, support and for just being there.

This work was kindly supported by the Sigrid Juselius Foundation, Finnish Cultural Foundation of Northern Savo and Aarne ja Aili Turusen Säätiö.

Kuopio, September 2009

Kimmo Jokivarsi

ABBREVIATIONS

2SX	two-site exchange
ADC	apparent diffusion coefficient
AFP	adiabatic full passage
AHP	adiabatic half passage
APT	amide proton transfer
APTR	amide proton transfer ratio
ASL	arterial spin labeling
ATP	adenosine triphosphate
b	diffusion weighting
B_0	external magnetic field
B_1	magnetic field created by a radio frequency field
$B_{1,SL}$	magnetic
B_{eff}	effective magnetic field
BBB	blood brain barrier
BOLD	blood oxygen level dependent
Ca^{2+}	calcium ion
CASL	continuous arterial spin labeling
CBF	cerebral blood flow
CBV	cerebral blood volume
Cl^-	chloride ion
$CMRO_2$	cerebral metabolic rate of oxygen
CNR	contrast to noise ratio
CPMG	Carr-Purcell-Meiboom-Gill
CPP	cerebral perfusion pressure
CT	computer tomography
CVA	cerebral vascular accident
CW	continuous wave
δ	gradient duration
Δ	time between gradient pulses
ΔE	energy difference
$\Delta\omega$	off-resonance component of the effective spin lock field frequency
D	diffusion constant
D_{av}	1/3 of the trace of the diffusion tensor
DCE	dynamic contrast enhanced
DNA	deoxyribonucleic acid
DSC	dynamic susceptibility contrast
DTI	diffusion tensor imaging
DWI	diffusion weighted imaging
EAA	excitatory amino acid
ECA	external carotid artery
EPI	echo-planar imaging
ETL	echo train length

FASTMAP	fast automatic shimming technique by mapping along projections
FID	free induction decay
fMRI	functional magnetic resonance imaging
FOV	field of view
FSE	fast spin echo
γ	gyromagnetic ratio
G	gradient amplitude
Gd-DTPA	gadolinium(III)diethyltriaminepentaacetic acid
GE, GRE	gradient echo, gradient recalled echo
h	Planck's constant
Hb	hemoglobin
HS	hyperbolic secant
ICA	internal carotid artery
IR	inversion recovery
K^+	potassium ion
k	Boltzmann constant
k_{ex}	exchange rate constant
λ	tortuosity coefficient
Lac	lactate
LASER	localization by adiabatic selective refocusing
μ	magnetic dipole moment
m	mass of a particle
M	magnetization
MCA	middle cerebral artery
MCAo	middle cerebral artery occlusion
MR	magnetic resonance
MRA	magnetic resonance angiography
MRI	magnetic resonance imaging
MRS	magnetic resonance spectroscopy
MT	magnetization transfer
MTR	magnetization transfer ratio
MTT	mean transit time
N_2O	nitrous oxide
Na^+	sodium ion
NAA	N-acetyl aspartate
NMDA	N-methyl-D-aspartic acid
NMR	nuclear magnetic resonance
OER	oxygen extraction ratio
P_A, P_B	pool size i.e. fractional spin population
PASL	pulsed arterial spin labeling
pCO_2	partial pressure of carbon dioxide
PCr	phosphocreatine
PD	proton density
PET	positron emission tomography

PFA	paraformaldehyde
pH_i	intracellular pH
pO_2	partial pressure of oxygen
ppm	parts per million
PTR	proton transfer ratio
PWI	perfusion weighted imaging
q	charge of a particle
r	correlation
R	relaxation rate (R_1=1/T_1)
RF	radio frequency
ROI	region of interest
ROS	reactive oxygen species
rt-PA	recombinant tissue plasminogen activator
S	signal intensity or spin quantum number
SAR	specific absorption rate
SD	standard deviation
SE	spin echo
SEM	standard error of mean
SL	spin lock
SNR	signal to noise ratio
θ	angle between effective magnetic field and transverse plane
τ	time delay
τ_c	correlation time
τ_{CPMG}	delay between refocusing pulses
τ_{ex}	exchange time
T_1	longitudinal (spin-lattice) relaxation time
$T_{1\rho}$	longitudinal relaxation time in rotating reference frame
T_2	transverse (spin-spin) relaxation time
T_2*	effective transverse relaxation time
$T_{2\rho}$	transverse relaxation time in rotating reference frame
TE	time to echo
TI	inversion time
TIA	transient ischemic attack
TOF	time of flight
TR	time to repetition
T_{SL}	spin lock time
TTP	time to peak
WHO	World Health Organization
ω	angular precession frequency
ω_0	Larmor frequency
ω_{eff}	effective spin lock field frequency
$\omega_{1,SL}$	on-resonance component of the effective spin lock field frequency

LIST OF ORIGINAL PUBLICATIONS

This thesis is based on the following publications referred to by their corresponding Roman numerals:

I **Jokivarsi KT**, Gröhn HI, Gröhn OH, Kauppinen RA. "Proton transfer ratio, lactate, and intracellular pH in acute cerebral ischemia." *Magn Reson Med. 2007 Apr;57(4):647-53.*

II Jolkkonen J, **Jokivarsi K**, Laitinen T, Gröhn O. "Subacute hemorrhage and resolution of edema in Rose Bengal stroke model in rats coincides with improved sensorimotor functions." *Neurosci Lett. 2007 Nov 27;428(2-3):99-102.*

III **Jokivarsi KT**, Niskanen JP, Michaeli S, Gröhn HI, Garwood M, Kauppinen RA, Gröhn OH. "Quantitative assessment of water pools by T1rho and T2rho MRI in acute cerebral ischemia of the rat." *J Cereb Blood Flow Metab. 2009 Jan;29(1):206-16.*

IV **Jokivarsi KT**, Hiltunen Y, Tuunanen P, Kauppinen R, Gröhn O. "Correlating Tissue Outcome with Quantitative Multiparametric MRI of Acute Cerebral Ischemia in Rats" *Submitted*

TABLE OF CONTENTS

1 INTRODUCTION **17**

2 REVIEW OF LITERATURE **19**

2.1 Cerebral ischemia 19
2.1.1 Acute cerebral ischemia *19*
2.1.2 Ischemic changes in tissue *20*
2.1.3 Molecular motion and interactions of water in the context of MRI contrasts *25*
2.2 MR techniques for detection of cerebral ischemia 30
2.2.1 Nuclear magnetization and magnetic resonance imaging *30*
2.2.2 T_1 and T_2 relaxation times *33*
2.2.3 Rotating frame, $T_{1\rho}$ and $T_{2\rho}$ *36*
2.2.4 Blood Oxygenation Level-Dependent MRI *39*
2.2.5 Diffusion MRI *39*
2.2.6 Perfusion *42*
2.2.7 Magnetization transfer and Z-spectroscopy *45*
2.2.8 Amide Proton Transfer Ratio and pH *46*
2.2.9 Magnetic Resonance Spectroscopy *46*
2.2.10 Multiparametric MRI *47*

3 AIMS OF THE STUDY **49**

4 MATERIALS AND METHODS **50**

4.1 Animals 50
4.1.1 Anesthesia and analgesia *50*
4.1.2 Ischemia *50*
4.1.3 Limb-placing test *51*
4.1.4 Histology *51*
4.2 NMR/MRI Methods 51
4.2.1 Hardware *51*
4.2.2 Data acquisition *52*
4.2.3 T_1 and T_2 ..... *52*
4.2.4 $T_{1\rho}$ and $T_{2\rho}$ *53*
4.2.5 Diffusion *53*
4.2.6 Perfusion, ASL *54*
4.2.7 Amide proton transfer ratio and intracellular pH *54*
4.2.8 Spectroscopy *54*
4.3 Data analysis 55

5 RESULTS **56**

5.1 Amide proton transfer ratio and pH in ischemia 56
5.2 Hemorrhage and ischemia development in the Rose Bengal model of stroke 57
5.3 Changes in water pools during ischemia 57
5.4 Correlating stroke lesion outcome with MRI data 58

6 DISCUSSION **60**

6.1 From individual MRI parameters 60
6.2 …through understanding the mechanism underpinning changes 63
6.3 …to multiparametric MR imaging 64
6.4 Future directions 65

7 SUMMARY AND CONCLUSIONS **66**

8 REFERENCES **67**

Appendix: Original publications (I-IV)

1 INTRODUCTION

Cerebral ischemia results from deficient blood supply to the brain. If not treated, this condition will rapidly lead to an injury of the central nervous system i.e. ischemic infarction and stroke. Stroke is the second most common cause of death after heart disease worldwide (Murray and Lopez, 1997) and according to the WHO statistics cerebrovascular disease was the cause of death of 5.7 million people in 2005 (Strong et al., 2007). Stroke is also a leading cause of long-term disabilities. In Finland around 12 000 people each year have cerebral infarction (Fogelholm and Baumann, 2002). In the US it is estimated to cause 550 000 hospitalizations and 150 000 deaths per year (Taylor et al., 1996). As a common debilitating disease it has been given several names such as brain attack, cerebral infarction, cerebral vascular accident (CVA) and apoplexy. With technological improvements and the subsequent better treatment and imaging methods, mortality due to stroke decreases, but the incidence rate within the aging population still remains the same. More and more people are being disabled by ischemic stroke. It is therefore a significant health burden both socially and economically for society. Better understanding of the disease, then more accurate diagnostics and better assessment of therapy is thus needed.

Currently several imaging techniques are available for stroke diagnosis. These include computer tomography (CT), positron emission tomography (PET), and magnetic resonance imaging (MRI). CT is a routine technique in patient management, but it lacks sensitivity and specificity to acute stroke, still it is a well established tool in clinics to detect hemorrhage in stroke patients. PET on the other hand produces quantitative images from cerebral hemodynamics and metabolism and is extremely sensitive in absolute terms. Unfortunately the drawbacks with PET, including low spatial resolution and need of radiolabeled markers, renders it less practical for routine imaging of acute stroke. Recent developments in MRI techniques have increased the sensitivity of this clinical imaging modality for detection of acute stroke. It is well established that diffusion (the translational Brownian motion of water molecules in tissue) and perfusion (the rate of blood delivered to tissue) change nearly instantly following the onset of ischemia. For MRI, acute changes in brain water dynamics due to ischemia provide excellent contrast making MRI a very sensitive tool for early stroke detection, well before the subtle changes in tissue morphology are evident.

Using established and investigational MRI contrasts, acute infarct can be visualized within minutes from the drop of blood flow below the ischemic threshold. However, the dynamic changes in brain water physico-chemistry during ischemia are complex. Largely due to these factors, current MRI contrasts can visualize only a fraction of biophysical processes in brain tissue that are launched by ischemia. To complement the conventional stroke MRI contrasts, i.e. diffusion, perfusion and T_2, novel contrasts are under investigation. Alas, as for the moment there are no proven and clinically accepted pharmacological treatments for stroke, other than dissolving the blood clot by

thrombolysis, there is no present clinical need for more specialized imaging techniques. Still MRI has unexplored potentials as an advanced imaging technique as it can exploit the water proton dynamics on the changing tissue microenvironment for instance during the developing ischemic stroke. There are several ongoing studies to understand the biochemical and biophysical processes in cerebral ischemia (Cho and Kim, 2009; Dietz et al., 2009; Niizuma et al., 2009). This thesis is one small part of the big effort to increase the knowledge and improve the tools for diagnosis of this common but still not well understood disease.

2 REVIEW OF LITERATURE

2.1 Cerebral ischemia

2.1.1 Acute cerebral ischemia

Under physiological conditions oxygenated blood is supplied to tissue by arteries and oxygen then diffusively exchanges into tissue at the capillary bed. Deoxygenated blood flows out of the brain through the venous network back to the lungs to be reoxygenated. A diminished supply of blood to tissue results in ischemia. A lack of oxygen (and glucose) will lead to failure of the energy-dependent processes and thereafter to stroke. Acute stroke is essentially a sudden loss of brain activity due to lack of energy, or more precisely a lack of energy substrates glucose and oxygen (Siesjö, 1992).

About 80% of strokes are caused by cerebral ischemia. This is often due to a blood clot (thrombus), a plug of coagulated platelets originating from the heart or carotid artery bifurcation that has made its way to an intracranial artery. Other causes for stroke include hemorrhage and postoperative hypotension. Also, transient ischemic attack (TIA) can cause small stroke-like symptoms as an artery is occluded temporarily. A recent consensus states that TIA usually resolves within an hour and unlike in stroke there is no permanent damage to the brain (Easton et al., 2009).

The main therapeutic strategies proposed for acute stroke treatment are to recanalize the occluded artery or to protect the brain tissue in risk of dying until the ischemia is resolved. Several strategies for treatment of ischemic damage have been suggested and are under investigation, such as clinical hypothermia (Diller and Zhu, 2009; Jiang et al., 1994). New techniques are emerging, but so far only one therapy method has been proven to be effective and is in clinical use. That is the intravenous thrombolysis with recombinant tissue plasminogen activator (rt-PA). The effectiveness of this therapy in reducing the infarct size is time-dependent (Zivin et al., 1988). The therapeutic window for salvaging the tissue at risk is only a few, typically three hours. Nowadays, if the patient is diagnosed within this time window from the onset of symptoms, and hemorrhage can be excluded, the blockage can be treated (del Zoppo et al., 1992). Widening of this time window has also been suggested to 4.5h (Hacke et al., 2008; Martinez-Sanchez et al., 2007) as there may be salvageable tissue beyond the 3h window (Markus et al., 2004). Apart from improved pharmaceutical methods for thrombolysis and finding effective methods for neuroprotection other progress is then needed in the imaging methods, to select appropriate treatments for patients.

Several experimental animal models of cerebral ischemia have been developed to study the two main ischemia types, i.e. transient and permanent ischemia. The experimental models provide valuable information about the pathophysiology of ischemic brain damage. They give a controlled environment to assess the development of a stroke lesion and to test new potentially therapeutic agents for stroke treatment. With experimental animal models intervention of stroke development has worked with ion channel blockers (Okada et al., 2006), excitatory amino acid antagonists (Kimelberg et al., 2004) and free radical scavengers (Slemmer et al., 2008). Functional improvement has also been obtained after stem cell transplantation in animal models of stroke (Borlongan et al., 1998; Li et al., 2000) and clinical trials have been followed by some positive results (Kondziolka et al., 2000). Unfortunately, the over 700 therapeutic agents that have been studied and been successful in animal trials have failed in human trials (del Zoppo, 1998; Durukan and Tatlisumak, 2007). More appropriate animal models are clearly needed. Despite these shortcomings imaging of different animal models has been essential in the development of MR imaging techniques. Furthermore, imaging is and will be an important tool to guide the experimental evaluation of drugs and for tracking transplanted cells (Modo et al., 2004).

Much work has been directed towards understanding the biochemistry and molecular biology of neuronal damage (Kochanek et al., 2008; Sims and Zaidan, 1995). However, not only the neurons are essential in supporting the functioning brain and preventing and/or promoting the ischemic injury nor are they the only damaged cells during ischemia. An increasing amount of data show an important role of astrocytes in the ischemic damage evolution (Dienel and Hertz, 2005; Takano et al., 2009; Trendelenburg and Dirnagl, 2005). As the astrocytes perform several transportation and regulation functions in the brain, impairment in any of these may result in hindrance of neuronal function. On the other hand, astrocytes are more resistant to ischemia and other insults than neurons. They can continue producing adenosine triphosphate (ATP) during glucose deprivation due to their glycogen reserve (Dringen et al., 1993) and can protect against ischemic injury during incomplete ischemia (Rossi et al., 2007; Swanson et al., 1994; Swanson et al., 1997). Also microglia is a possible contributor to ischemic damage (Denes et al., 2008). Therefore astrocytes, glial cells and neurons both themselves and together will constitute therapeutic targets for novel pharmaceutical therapies.

2.1.2 Ischemic changes in tissue

2.1.2.1 Hemodynamic regulation and energy dependence

Under normal physiological conditions blood flow is tightly regulated to preserve the oxygen and glucose supply and thus the energy production in cells. In the ischemic brain oxygen is quickly

exhausted, and eventually so is glucose. ATP, however, may be preserved for a longer period of time due to secondary metabolic pathways. Cerebral perfusion pressure (CPP) and thus cerebral blood flow (CBF) can decline due to a stenosis in the carotid artery, vertebral artery or one of their intracranial branches (Powers et al., 1985; White and Markus, 1997). To increase the amount of incoming blood autoregulated capillary dilatation can reduce the vascular resistance and thus increase cerebral blood volume (CBV). Also, the oxygen extraction ratio (OER), representing the amount of oxygen transferred from blood to tissue, increases in capillaries to preserve normal oxygen metabolism. OER is defined as

$$OER = \frac{CMRO_2}{[Hb_{tot}] \cdot CBF \cdot Y_a}, \quad (1)$$

where $CMRO_2$ is the cerebral metabolic rate of oxygen consumption, $[Hb_{tot}]$ the hemoglobin concentration and Y_a the arterial oxygen saturation (i.e. the fraction of arterial oxygenated hemoglobin). Under physiological conditions OER in unstimulated brain is 0.36-0.42 (Cohen et al., 1967). Further decrease in the blood supply eventually causes reduction in the amount of oxygen and glucose delivered to tissue cells. This is followed by decrease in the production of ATP, which is the main chemical energy source for the cell (Sokoloff, 1989).

To maintain cell functionality, a continuous supply of oxygen and glucose is needed. ATP is mainly produced by the oxidative glucose metabolism, aerobic glycolysis feeding substrates for the oxidative phosphorylation. Under anaerobic conditions i.e. when oxygen supply is insufficient, carbohydrate (glucose) is transformed in anaerobic glycolysis to ATP and lactate (Hochachka and Mommsen, 1983; Huckabee, 1958; Katsura et al., 1991). During complete ischemia in the core of the lesion the cells can survive about 2-3 minutes before cellular damage. Still in some ischemic situations cells can survive hours or days due to collateral perfusion (Dereski et al., 1993).

When capillaries have dilated to their maximum size CBF will start to decay rapidly and OER increases (CPP under 60 mmHg). CBV increases during the autoregulatory phase of vasodilatation and collapses after the CPP break point of about 20 mmHg (Ferrari et al., 1992; Grubb et al., 1973; Schumann et al., 1998; Zaharchuk et al., 1999). Oxygen metabolism ($CMRO_2$) remains unchanged due to vasodilatation and increased OER as long as the autoregulatory system is functional (Schumann et al., 1998; Zaharchuk et al., 1999). OER can increase close to 100% as the flow in capillaries slows down and the partial pressure of oxygen pressure at half-saturation (P_{50}) of hemoglobin is lowered (Popel and Gross, 1979). The high OER (Grubb et al., 1998; Yamauchi et al., 1996) with increased CBV (Derdeyn et al., 2002) thus shows that the hemodynamic autoregulation is closing its limit and there is a risk of infarction. Also, when CBF drops below the threshold of energy failure this causes a reduction on water diffusion (Busza et al., 1992) (see chapter 2.2.5).

One major cause for tissue damage is the reperfusion injury (Aronowski et al., 1997). During ischemia tissues will adapt to the anaerobic situation (Carden and Granger, 2000). During reperfusion there is a sudden excess of oxygen that leads to macrophage activation and production of oxide radicals (ROS) (Granger and Korthuis, 1995). This may lead to disruption of the blood brain barrier, hemorrhagic transformation and/or brain edema.

2.1.2.2 CBF thresholds for ischemia

In the ischemic core the CBF is reduced close to zero. The surrounding border zone with lowered perfusion is called the penumbra, which is dependent on the collateral circulation. It is a structurally intact viable region at risk of going into infarction. Already it is functionally impaired, but maintains cell polarization, i.e. it is between the two CBF thresholds: the electrical failure of the cell and failure of the ion-pumps (Astrup et al., 1981; Heiss, 1983; Hossmann, 1994; Siesjö, 1992).

Powers and coworkers (Powers et al., 1987) showed that when the automatic vasodilatation is working during a hemodynamic impairment only the CBV (or CBV/CBF) increases, but when the autoregulation fails, CBF is reduced and OER increased. This has been shown in patients with carotid artery disease (Yamauchi et al., 1996) and animal models (Dirnagl and Pulsinelli, 1990; Verhaegen et al., 1993). Decrease of cerebral blood flow (CBF) to 50-60% of the normal physiological values (i.e. below 35ml/100g/min) leads to cessation on protein synthesis (Mies et al., 1991). At 30-40% the neural functions are lost and tissue is at risk of irreversible infarction. If CBF falls below 20% of normal values irreversible cell death will occur within minutes. The experimental threshold value for CBF is about 20 ml/100g/min under which symptoms of ischemic stroke start to emerge, such as cessation of neuronal activity (Astrup et al., 1977). Figure 1 shows a schematic view of CBF thresholds for various processes.

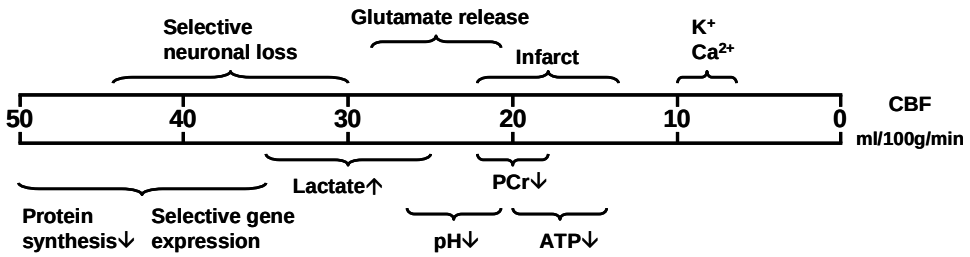

Figure 1: CBF thresholds for the induction of functional, metabolic and histological lesions during cerebral ischemia. PCr = phosphocreatine. (Modified from Hossmann 1994.)

2.1.2.3 Acute changes

Under physiological conditions there is an active energy-dependent maintenance of concentration difference of ions between the extra- and intracellular spaces. The membrane ion pumps on the cell surface need ATP to maintain these electrolyte concentration gradients and the fluid distribution that follows the osmolytic pressure.

Membrane depolarization of cells is induced due to the failure of the Na^+/K^+-ATPase pump that maintains the transmembrane gradients and takes care of the active influx and efflux of ions. Sodium (Na^+) needs to be pumped out of and potassium (K^+) into the cell, to keep the ionic homeostasis. Inside an ischemic lesion the central oxygen compromised area has insufficient energy supply from the ATP to maintain its cell energy pumps. Within a few minutes the amount of intracellular Na^+, chloride (Cl^-) and calcium (Ca^{2+}) increases. In the extracellular (interstitial) space there is increase in K^+ and lowered Na^+, Cl^- and Ca^{2+} concentrations (Hansen and Zeuthen, 1981). The homeostasis is lost and this will lead to neuronal depolarization i.e. the loss of membrane potential (Astrup et al., 1977). This disruption in the ion balance starts the cytotoxic edema, the osmotic influx of fluid (water) into the cell that leads to cellular swelling.

Neurons are very sensitive to ischemia, and the elevation of intracellular Ca^{2+} is one of the central causes of ischemic injury to neuronal cells (Kristian and Siesjo, 1998). Ischemia induced cell membrane depolarization causes an increased release of excitatory amino acids (EAA), such as glutamate. This activates NMDA and metabotropic glutamate receptors, causing the so called excitotoxicity. By enabling the Ca^{2+} channels and triggering the Ca^{2+} release from the intracellular stores and structures this leads to the increase of Ca^{2+} inside the cell. The excess intracellular Ca^{2+} activates several processes (e.g. proteases and phosholipases) and causes the production of reactive oxygen species (ROS). This will start the destruction of the cell cytoskeleton, membranes and DNA. This excess Ca^{2+} can trigger both apoptotic and necrotic cell death.

Cell deaths can be categorized loosely to two types. Necrotic death often results after a quick and total loss of energy and oxygen. The cells swell and lose their cellular structure. The cytoplasmic contents are released into the extracellular space leading to inflammation (among others, destruction by enzymes). After a short exposure to ischemia cells may undergo a controlled elimination, i.e. apoptosis. Apoptosis requires energy and involves activation of apoptotic pathways (Broughton et al., 2009; Dirnagl et al., 1999). It features chromatin aggregation, nuclear and cytoplasmic condensation and fragmentation of the cell to smaller membrane bound vesicles, the apoptotic bodies, containing intact organelles. The ischemic core is mostly driven to necrosis due to the loss of energy (Martin et al., 1998). Cells further away from the core suffering from anoxia but still having chemical energy left may end up in apoptotic death. At the border between lesion and surrounding normal tissue there is a band (penumbra) of heterogeneous population of viable,

apoptotic and necrotic cells. Studies show that a cell death is not necessarily clearly either of these but is rather on a continuum between the two extremes (Martin et al., 1998).

Once the damage becomes irreversible the neurons will swell, the glial cells start to fragment and the myelin sheaths degenerate. Many neuronal and glial cells along with blood vessels often end up in necrotic death during ischemia (Martin et al., 1998; Tsukada et al., 2001). Eventually the ischemic necrotic core will be dissolved and the area is filled with fluid. In time the swelling will cause morphological changes in the infarcting brain.

2.1.2.4 Delayed changes

In the blood brain barrier (BBB) the brain endothelial cells are tightly connected to each other. Tight junctions prevent passive diffusion and provide control over the exchange of molecules from blood to the brain tissue. In an ischemic injury the endothelial cells will suffer and the BBB starts to leak. As the protecting endothelial cells die unwanted compounds gain access to the extracellular space in the brain causing extra damage to cells. The hydrostatic pressure causes water to accumulate to the interstitial space causing the vasogenic edema (Klatzo, 1967). Further tissue degeneration also increases the extracellular space and increases the edema. Further increase in the intracranial pressure may also lead to secondary ischemia. Effects of hypoxic ischemia to BBB is reviewed by Kaur and Ling (Kaur and Ling, 2008).

Ischemia causes inflammatory responses as well as alterations in gene regulation and expression. Transformation of carbohydrate in anaerobic glycolysis leads to accumulation of lactic acid, non-neutralized protons in the cell and further to drop of intracellular pH (Behar et al., 1989; Siesjö, 1992; Smith et al., 1986). Low pH worsens the damage caused by a transient ischemia due to the activation of lipases and proteases (Siesjö et al., 1990). Free radical formation increases during ischemia, in the absence of oxygen and hindered scavenging, and especially during reperfusion. The reactive oxygen species (ROS) react easily and cause lipid peroxidation and irreversible damage to proteins, DNA and further hamper cellular functions. Inflammation following the ischemic damage is reviewed by Amantea et al. (Amantea et al., 2009).

Around the ischemic core the recurrent waves of depolarization is suggested to be a cause of the eventual loss of energy and turning of the surrounding tissue into lesional core (Hansen and Lauritzen, 1984; Takano et al., 1996). These spreading depression-like depolarizations may be due to elevated extracellular K^+ levels and increased glutamate release at the border of the lesion core (Branston et al., 1977). In the core the ion homeostasis is lost due to low CBF and the depolarization is permanent. Figure 2 shows a schematic view of mechanisms and their impact

values that take place during focal ischemia from the early excitotoxicity to the late effects of inflammation and apoptosis (Dirnagl et al., 1999).

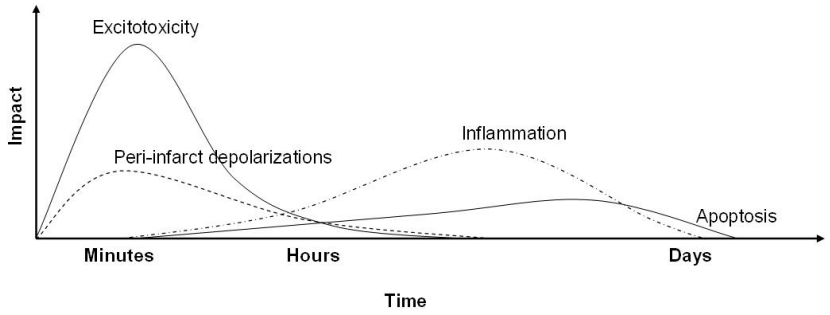

Figure 2: Time curves of the impact of various deleterious processes during focal cerebral ischemia. (Adapted from Dirnagl et al. 1999.)

Experimental models have demonstrated that the ischemic lesion expands in time during the first 2 hours after middle cerebral artery occlusion (MCAo) in rats and cats (Hoehn-Berlage et al., 1995; Miyabe et al., 1996; Roussel et al., 1994). This expansion continues up to 48 hours due to the vasogenic edema (Verheul et al., 1992). Also the experimental models of MCAo often show the lesion first in striatum and then expanding to cortex (Reith et al., 1995). Often a delayed cell death corresponds with an apoptotic cell death (Beilharz et al., 1995; Nitatori et al., 1995; Tortosa et al., 1994).

2.1.3 Molecular motion and interactions of water in the context of MRI contrasts

A water molecule consists of one oxygen and two hydrogen atoms. Electronegativity difference between these atoms causes the nonuniform distribution of the electron cloud around the nuclei and makes the water molecule an electric dipole. The surrounding environment of a spinning nucleus is called the lattice - even in liquids. Each molecule is in constant motion that consists of vibration, rotation and translation. The motion of nuclei in a lattice creates local magnetic field fluctuations. Molecules rapidly change their motion due to collisions with each other. The time spent in one motional state is known as the correlation time τ_c.

Tissue water can be modeled to have three compartments according to their correlation times and interactions with macromolecules such as proteins (Diegel and Pintar, 1975; Finch and Homer, 1974; Grösch and Noack, 1976; Hazlewood et al., 1974; Knispel et al., 1974). In the free water pool (or bulk water) the water molecules are not in direct interaction with macromolecules. Here the correlation times are in the order of 10^{-12} s. In the structured water pool water molecules are not strongly bound to protein molecules but are either slightly bound with a hydrogen bond or in between the free and bound states, while the correlation times are from 10^{-9} to 10^{-11} s. In the bound water pool the water molecules are directly bound to protein molecules with hydrogen bonds that causes the correlation times from 10^{-3} to 10^{-9} s.

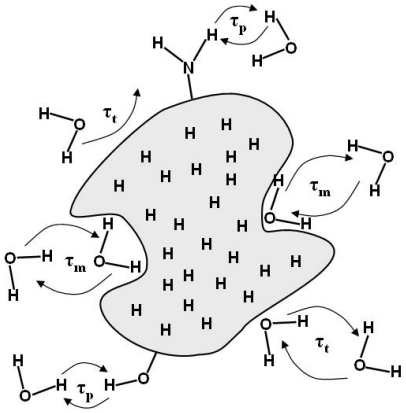

Figure 3: A schematic representation of the important interactions between water and a macromolecule. Correlation times are shown for proton exchange with ionisable groups (τ_p), exchange of a buried water molecule (τ_m) and transient collisions of a water molecule at the macromolecule surface (τ_t). (Modified from Bryant 1996).

When a water molecule comes to close proximity with a protein molecule these species interact in three different ways illustrated in Figure 3 (Bryant, 1996; Halle, 1999; Koenig and Brown III, 1994). In the first type, the water molecules near the surface of the protein molecule interact via transient collisions. The effect on relaxation times is minor as the correlation times for the translational water are very short and the dipole-dipole interactions are weak. In the second type the water protons are in close proximity and interacting through protons or chemical exchange with the ionisable groups of the protein, e.g. OH and NH groups and structured water molecules (Bryant, 1996). The water proton binds covalently to the protein and replaces a labile proton. The released proton then bonds covalently to the water molecule. The third type of interaction is the whole molecule interaction, where the water molecule binds to the surface of the protein with hydrogen bonds. In cross-relaxation, the spin of a nucleus changes state as a consequence of a spin change in

the dipolar coupled partner. Due to the long duration of the bonding times, cross-relaxation occurs via dipole-dipole interactions.

There is a constant exchange in tissue between water molecules and macromolecules. There are different time scales for this rate of exchange. In fast exchanging systems the resulting relaxation is mono-exponential, whereas in slow and intermediate exchange the observed signal decay is non-monoexponential. For fast exchange the exchange time τ_{ex} is

$$\tau_{ex} = \frac{1}{k_{ex}} << (\delta\omega)^{-1}, \tag{2}$$

where $\delta\omega$ is the so called chemical shift difference (see 2.2.9) and k_{ex} the exchange rate constant.
If two exchanging pools are in equilibrium exchange, then

$$\tau_{ex} = \frac{P_A}{k_{-1}} = \frac{P_B}{k_1}, \tag{3}$$

where $P_{A,B}$ are the water pool sizes (fractional spin populations), where P_A=1-P_B, and k_1 and k_{-1} are the forward and backward exchange rate constants between the sites *A* and *B*.

During ischemic stroke there are several factors that cause changes in the distribution of tissue water and the overall tissue water content. In the hyperacute phase the intracellular water content increases due to cytotoxic edema, which also causes a decrease in the extracellular space. The redistribution of water from the extracellular space to the more viscous and structured intracellular space has been suggested to be a cause of decreased diffusion in tissue during ischemia (Benveniste et al., 1992; Hasegawa et al., 1996; Moseley et al., 1990; van Gelderen et al., 1994; Verheul et al., 1994). However, according to Duong et al. (Duong et al., 1998) the water signals from both the extra- and intracellular compartments are similar. Therefore, a water shift of a few percent could not significantly reduce the total diffusion. The residence time of water in the extracellular space is long compared to the intracellular water (around 0.55 and 0.12 s respectively) and the exchange between compartments is slow (Quirk et al., 2003), therefore the exchange should not have an effect on the diffusion change during ischemia (Clark and Le Bihan, 2000; Duong et al., 1998). The cytotoxic edema also leads to an increase in the extracellular tortuosity, i.e. more constrained and complex diffusional path for the molecule (Duong et al., 1998). But this makes only a small contribution to the total decline of the water diffusion as the extracellular space comprises about 10-20% of the total volume during cytotoxic edema.

Another factor causing increased diffusion is the elevated intracellular viscosity (Wick et al., 1995). This may be due to activation of proteases and phospholipases that cause degradation and destruction of intracellular structures (Inuzuka et al., 1990). Also a minor factor in the diffusion change is the reduction of the water permeability in the cell membranes (Latour et al., 1994; Szafer et al., 1995). Structural and functional cytosolic changes, such as swelling of organelles (mitochondria), increase in the amount of membranes and fibrillary structures and disorganization

of the cytoskeleton affect the intracellular diffusion. The disruption of the structure of macromolecules may increase their interaction (binding) to water and thus affect water mobility. Furthermore, an energy dependent circulatory system has been proposed as an intracellular metabolic function and transport system that circulates the cytoplasmic fluid for internal cell perfusion (Hochachka, 1999; Wheatley, 1985). Energy failure causes the cessation of active intracellular streaming and leads to an injury to the cell. This has been suggested to be a major factor contributing to the decrease of the diffusion (Duong et al., 1998).

A temperature decrease of a few degrees has only a small effect on the diffusion, but a strong effect on the damage by decreasing the damage by hypothermia or increasing the damage by hyperthermia (Busto et al., 1987; Reith et al., 1996; Schwab et al., 1998). This has been reviewed by Krieger and Yenari (Krieger and Yenari, 2004). Temperature drop also slows down exchange processes and thus affects relaxation times (Bottomley et al., 1984).

Table 1: MRI parameters, their commonplace acquisition techniques, origin of contrast and significance in stroke assessment. (For references, please, see text.)

	MRI Parameter	Technique(s)	Contrast due to	Significance in stroke
Relaxation	T_1	Inversion recovery (IR) or saturation recovery (SR)	Altered overall water content and possibly changes in loosely bound (correlation time in order of 10^{-9} s) water fraction	A small increase due to cessation of blood flow, a more pronounced increase associated with vasogenic edema
	T_2	Spin echo (SE), CPMG	Early shortening due to negative BOLD effect. Subsequent increase chiefly due to vasogenic edema with possible contribution from breakdown of intracellular structures	Hyperacute decrease associated with reversible ischemia, whereas prolongation associated with irreversible damage
	T_2*	Gradient echo (GRE)	Changes in magnetic susceptibility	Hemorrhage marker
	$T_{1\rho}$ ($T_{2\rho}$)	On-resonance spin lock (SL)	Change in the water-macromolecule interaction and overall water content in tissue	Increases from the first minute after ischemia. MRI marker of irreversible damage
Diffusion	D_{av}	Diffusion weighted imaging	Biological and biophysical mechanisms debated. Acute decrease associated predominantly with depolarisation of cells, cytotoxic edema and slow down of exchange between intracellular and extracellular space. Increase due to breakdown of the cellular structures	Important marker of hyperacute ischemia. Early decrease does not necessarily mean irreversible ischemia. Increased diffusion associated with chronic irreversible lesion
Hemodynamics	**CBF**	Dynamic susceptibility contrast (DSC) or arterial spin labeling (ASL)	Change in blood flow	Declines due to occluded blood vessel. Diffusion-perfusion mismatch a commonly considered signature of tissue at risk
	CBV	DSC or intravascular contrast agent	Change in blood volume and blood flow	Signal increases during vasodilatation, where tissue is deprived of oxygen to maximize oxygen delivery. Decreased in severe ischemia
	MTT	DSC	Delayed transit time of contrast agent	Prolonged transit time shows hindered blood flow
Magnetization transfer	**MTR**	Offset saturation	Magnetization interaction between bound and bulk water. Changes due to protein water interaction, water pool sizes, pH, and T_1 relaxation times of the pools involved	Decreases due to macromolecule breakdown and vasogenic edema
	APTR	Offset saturation at amide proton resonance frequency	Interaction between protein amide group protons and bulk water. Potential marker for penumbra	Decreases mainly due to acidification, but also affected by temperature and other physicochemical factors, such as MT
Proton Density		Proton density weighted imaging	Overall water content in tissue	Increases in vasogenic edema during the irreversible phase of stroke

2.2 MR techniques for detection of cerebral ischemia

The use of nuclear magnetism has gone a long way since the first descriptions of the mysterious lodestones by the Greek Thales around 600 B.C. The discovery of nuclear magnetic resonance (NMR) in 1940's (Bloch et al., 1946; Purcell et al., 1946) gave the foundation for the advent of magnetic resonance imaging (MRI) in the 1970's. Since then MRI has become an important experimental and clinical tool and during the last decades greatly enhanced the clinical assessment of location and severity of cerebral stroke. Being a non-invasive technique it is well suited for *in vivo* studies both clinically and experimentally. Different MRI techniques can give detailed information about the different aspects of the hemodynamic and pathological changes in the ischemic tissue during the evolution of an acute stroke. In experimental studies of ischemia one of the remaining challenges for MRI is to define the recoverable penumbra that can potentially be treated and separate it from the irreversibly damaged ischemic core.

The ^{1}H MR signal from tissue is largely dependent on proton density. As most of the body consists of water the measured MR signal is mainly from water and thus gives information of water in different states (pools) in tissue. Relaxation times depend on the correlation time distribution in tissue and therefore reflect the state of the water in tissue. In a solution of pure water ("bulk water") relaxation times are longer and in bound state they are shorter due to interactions with macromolecules. As the water content, mobility of the molecules in lattice or the ratio of the water pools changes (e.g. due to ischemic damage) so change the relaxation times.

In experimental and clinical studies MR can be used in two distinct modes: (a) sampling the spectrum of a biochemical compounds (MR spectroscopy, MRS) or (b) determining the spatial distribution of water in tissue (MRI). In MRI the main physical properties that are exploited to produce contrast are magnetization relaxation processes, magnetization transfer (MT) processes between water molecules in the different pools and molecular displacement due to diffusion or flow. A list of MRI techniques with their relevance to stroke imaging is presented in Table 1.

2.2.1 Nuclear magnetization and magnetic resonance imaging

Of the human body roughly 70% is water. Each cubic centimeter of water has about $3.76*10^{22}$ water molecules and each of these water molecules consists of one oxygen (^{16}O) and two covalently bound hydrogen atoms (^{1}H). Atomic nuclei that have an odd number of protons and/or neutrons (e.g. ^{1}H, ^{13}C and ^{31}P) have a virtual angular momentum called spin. Thus the hydrogen ion i.e. proton is a positively charged particle with this intrinsic property. Thermal (Brownian) motion

causes molecules to have random orientation and thus there is no net magnetic field of the spin system. An external magnetic field B_0 applies a torque on the spin of the charged particle causing it to orientate parallel or anti-parallel to B_0 and to rotate around it at a certain frequency (Rabi et al., 1938). The relationship between the spin and the magnetic property of the particle is called the gyromagnetic ratio γ. In classical terms it can be defined roughly as

$$\gamma = q/2m\,, \tag{4}$$

where q is the charge and m the mass of the particle. For hydrogen ^{1}H (proton) γ is 42.57 MHz/T. The spinning of a charged particle gives it a magnetic dipole moment μ defined as

$$\mu = \gamma S = \left|\gamma m_s \hbar\right|,\ \hbar = h/2\pi\,, \tag{5}$$

where S is the spin quantum number and m_s is the magnetic quantum number, 1/2 and ±1/2 for a proton respectively, and h is the Planck's constant. In an external field these spins will be oriented either parallel or anti-parallel to the field, thus defining the energy state of the spin. For spin 1/2 nuclei there are two energy levels that depend on the external magnetic field. The energy difference between these energy states ΔE is

$$\Delta E = \hbar\omega_0 = \gamma\hbar B_0\,, \tag{6}$$

The energy at the parallel state is lower and by absorbing an energy quantum with a frequency of ω_0 the spin can make transitions to the higher energy state. The spins have a tendency to get to the lower energy state and thus there is a slight excess of spins aligned parallel to the B_0. The ratio between the numbers of spins between these states is given by the Bolzmann equation

$$\frac{N_\alpha}{N_\beta} = e^{-\Delta E/kT} = e^{-\gamma\hbar B_0/kT}\,, \tag{7}$$

where N_α and N_β are the number of nuclei in the different energy states or spin orientation, ΔE is the energy difference between the states, k is the Boltzmann constant ($1.38*10^{-23}$ J/K) and T is the temperature in Kelvin. The small excess of spins in the lower energy parallel state causes the tiny macroscopic magnetization M_0 that can be measured by NMR.

In classical terms, the spinning of a particle causes the spinning axis to rotate or precess about an axis. Similarly the nuclear spin quantity causes the virtual spinning axis to precess about the magnetic field B_0 with a specific frequency known as Larmor frequency that depends on the external field strength. The precession frequency ν can be defined as

$$\nu = \frac{\Delta E}{h} = \frac{\gamma B_0}{2\pi}, \tag{8}$$

where ΔE is the difference between the two energy states. The angular precession frequency ω is then

$$\omega = \gamma B_0\,. \tag{9}$$

The frequency of the precessing proton is therefore the same as the frequency of the radiation required to cause a transition between the two states. As ω is usually in the radio frequency (RF) range, the transitions between states can be induced with RF-pulses.

The random orientation of individual spins causes the net magnetization (vector sum of the individual spins) M_0 to be virtually zero. In an external magnetic field, B_0, each spin is slightly affected and the Bolzmann distribution of the spins leads to a non-zero M_0 that is parallel to the B_0. If an RF pulse is given to a spin system at their precession frequency it will induce changes between the spin states of the nuclei and each individual spin can change its state independently. The transmitting RF coil creates a magnetic field B_1 that is perpendicular to the B_0. By giving an appropriate amount of RF energy to the nuclei, i.e. applying a B_1 field at frequency ω, the M_0 can be tilted. The angle of this flip depends on intensity, waveform and duration of the RF pulse. This RF pulse causes phase coherence for the spins and by exciting the spins can even out the population difference between the states (90° pulse) or invert the populations (180° pulse). After a 90 degree pulse the magnetization will become tilted to the transverse plane (*xy*). After this excitation the spins start to return to the equilibrium state. The excited spins lose their energy and also their phase coherence, i.e. spin synchronicity. This relaxation of the nuclei is the return of the distribution of spins towards the Bolzmann distribution. The change from higher energy state to lower causes the nuclei to emit energy at the Larmor frequency. This precession of the M_0 during the return to the z-axis will induce an electrical signal with a frequency ω into the RF coil. This resulting signal is called the free induction decay (FID).

An external magnetic field gradient causes the precession frequency of a nucleus to become location dependent and therefore the location of the nucleus can be spatially coded. The resulting signal is a spectrum of the linear sum of the resonant frequencies. This signal can be recorded and stored in a 2D or 3D matrix called k-space. The k-space has as many points as the final image, but instead of spatial information it holds the frequency and phase information of the imaged slice. Each line in the k-space (in *x*-direction) generally represents one signal acquisition. The different frequencies of the nuclear spins due to field gradients cause phase dispersion. This dispersion depends on the strength and the length of the applied gradient. By using different gradient strengths in several acquisitions phase encoding can be created in the *y*-direction of the k-space, i.e. the phase encoding direction. As the data in k-space is in “spatial frequency” domain rather than in spatial (i.e. time) domain Fourier transformation is needed to convert the data to this spatial domain i.e. to a “conventional” MR image. However, the first 2D images were taken in 1973 by Lauterbur et al. using projection reconstruction as commonly used in X-ray imaging (Lauterbur, 1973). The 2D Fourier method was introduced only two years later (Kumar et al., 1975).

In MRI actual image contrast is a weighted combination of several contrasts, mainly T_1 and T_2 relaxation time constants, proton density in tissue and diffusion of the molecules. Different combinations of magnetic field gradient pulses, RF pulses and delays can be used to manipulate the M_0 to create different weighting between tissues that have different relaxation times.

In a conventional MR image the signal intensity (magnitude) of a point (i.e. pixel) comes mainly from the proton density and the relaxation times of water protons. There are two main parameters that are involved in the contrast formation of the MR image, namely time-to-echo (TE, echo time) and time-to-repetition (TR, repetition time). In a classic spin-echo experiment TE is the time from the 90 degree excitation pulse to the center of the echo. TR is the time between two repeated excitation pulses. In simple imaging sequences it is the time it takes to acquire one line in the k-space. By changing the TE and TR values the weighting between proton density, T_1 and T_2 will become altered. The total magnetization M and thus the signal intensity for each pixel in an image can be described as

$$M = M_0\left(1 - e^{-TR/T_1}\right)e^{-TE/T_2}. \quad (10)$$

For quantitative images, i.e. parameter maps representing one parameter such as relaxation constant T_1, several images have to be taken by changing one imaging parameter e.g. TR for each image. A map can be then calculated from these images by fitting an exponential function for each pixel.

2.2.2 T_1 and T_2 relaxation times

The contrast in MR images is due to different amount of signal loss in different tissues. This signal loss is partly due to nuclear relaxation characterized by two decay time constants: the longitudinal (T_1) and transversal (T_2) relaxation times. Several factors affect these relaxation times. These are dipole-dipole coupling, molecular motion, different interactions between water and macromolecules, local differences in magnetic susceptibility, temperature, pH and other physical and chemical conditions. Mostly the relaxation takes place through the direct dipole-dipole coupling, where the nuclear spins interact magnetically directly with each other through space. There are also indirect interactions between neighboring hydrogen atoms, when the nuclear spins interact through the bonding electrons between them (J-coupling).

T_1 is sensitive to rapid motion of the spin environment due to its sensitivity to small perturbations in the magnetic field that occur at the Larmor frequency, such as the motion of nearby spins. This makes T_1 also field dependent and it gets longer as the field increases. A common technique for T_1 measurement is the inversion recovery (IR) technique, where the magnetization M_0 is first inverted 180° followed by an inversion time (TI) and then a 90° pulse before the acquisition. The detected longitudinal magnetization M_z is

$$M_t = M_0(1 - 2e^{-TI/T_1}). \quad (11)$$

T_1 maps can be acquired by measuring the magnetization using several TIs for a recovery curve.

In the T_1-relaxation, or spin-lattice relaxation, the energy deposited by the RF excitation pulse dissipates into the surrounding tissue (or "lattice"). The time needed for this energy dissipation through dipole-dipole interaction is represented by the constant T_1:

$$\frac{1}{T_1} = K\left(\frac{\tau_c}{1+\omega_0^2\tau_c^2} + \frac{4\tau_c}{1+4\omega_0^2\tau_c^2}\right), \tag{12}$$

where τ_c is the correlation time representing the time needed for the molecule to rotate 1 radian in any direction and ω_0 is the angular frequency of the spin system around B_0, i.e. the Larmor frequency.

Another technique is the saturation recovery (SR) technique, where small flip pulses (flip angle 90° or less) are repeated in short intervals so that M_z is not completely recovered within the TR. Now the detected M_z is

$$M_t = M_0(1-e^{-TR/T_1}). \tag{13}$$

The transversal or spin-spin relaxation is characterized by the relaxation constant T_2. It is caused by time varying dipole-dipole interactions, where energy is not dissipated, but signal is lost due to dephasing of spins (the intrinsic T_2). This is defined as

$$\frac{1}{T_{2,\text{intr}}} = \frac{K}{2}\left(3\tau_c + \frac{5\tau_c}{1+\omega_0^2\tau_c^2} + \frac{2\tau_c}{1+4\omega_0^2\tau_c^2}\right). \tag{14}$$

Apart from this intrinsic relaxation T_2 it is also affected by diffusion and the exchange of protons. Then for T_2

$$\frac{1}{T_2} = \frac{1}{T_{2,\text{intr}}} + \frac{1}{T_{2,\text{diff}}} + \frac{1}{T_{2,\text{exch}}}. \tag{15}$$

The effective T_2 (T_2*) can be described as

$$\frac{1}{T_2^*} = \frac{1}{T_2} + \frac{1}{T_2'}, \tag{16}$$

where T_2' represents the reversible contribution of the coherent dephasing effects from fixed field changes. These are due to small changes in the tissue magnetic susceptibility or inhomogeneities of the external magnetic field. T_2* is the observed relaxation time of the free induction decay (FID) and is always shorter than T_2.

The intrinsic T_2 is relatively independent to field strength and it is more related to the slow variations (large τ_c) in the local magnetic environment. However, the apparent T_2 measured with spin echo sequence is related to the proton exchange of water molecules and local susceptibility inhomogeneities, which are heavily B_0 field dependent. As T_2 is also influenced by the same mechanisms as T_1, T_2 is always shorter than T_1 in tissue. In fast molecular motion regimes (bulk water, with small τ_c) T_2 is longer and starts to approach T_1. This is called the motional narrowing, as

line width is inversely proportional to T_2. In normal tissue, where slowly tumbling macromolecules are present, T_1 and T_2 can be used to obtain information about water dynamics in two different time scales.

Normally, before the excitation RF pulse there is no measurable transverse magnetization as the spins each have a random phase and thus cancel each other's contribution. To acquire signals with T_2 weighting the most basic sequence is the spin echo (SE) sequence originally demonstrated by Hahn (Hahn, 1950). In its common form a 90° pulse first flips the magnetization M_z to the transverse (*xy*) plane and creates phase coherence. The magnetization is left to dephase in the *xy*-plane for a time τ and a 180° RF pulse is then applied. This causes the spins that were dephased by the static field gradients to rephase (refocus) and thus create an echo after the time τ. The dynamic dephasing due to diffusion and exchange processes, the microscopic field fluctuations of the neighboring spins and dipole-dipole interactions, is not rephased. The time between the 90° pulse and the echo is the echo time (TE = 2τ) and the time between the successive 90° pulses is the repetition time (TR). As in equation (10) the relaxation curve for T_2 can be defined by

$$M_t = M_0 e^{-TE/T_2}. \tag{17}$$

There are several methods to measure T_2 and each of them gives a slightly different result due to their different sensitivity to diffusion and exchange effects (Allerhand and Gutowsky, 1964; Carr and Purcell, 1954). Two of the most common methods based on SE are the Hahn echo and Carr-Purcell-Meiboom-Gill (CPMG) multi-echo pulse technique (Meiboom and Gill, 1958). The Hahn echo method has a single refocusing pulse for one echo, whereas the CPMG method has a train of refocusing pulses that are separated by a delay (τ_{CPMG}) and the echo can be recorded after the whole train of pulses or after each refocusing pulse. By using repetitive 180° pulses (Carr and Purcell, 1954) the echo-to-echo amplitudes can be measured to assess the apparent T_2. By changing the delay the sensitivity to diffusion can be changed. The CPMG method gives an accurate T_2 weighting due to its insensitivity to diffusion owing to the short times between the 180° pulses. The CPMG sequence also has a phase shift of 90° relative to the excitation pulse that cancels out the errors in the 180° pulses. By short delay and several refocusing pulses the exchange contribution is minimized and in the Hahn echo method, when τ = TE the exchange contribution will have maximal effect.

Technically, to save time in imaging, multiple lines of the k-space can be acquired during one TR. Fast spin echo (FSE) sequences are done in a fraction of the time (usually 1/4-1/16) needed for a conventional T_2 weighted image. Echo train length (ETL) represents the number of k-space lines acquired per TR. For T_2* images gradient echo (GRE) can be used. It is excellent in detecting hemorrhage due to its high sensitivity to magnetic field inhomogeneities induced by paramagnetic breakdown products of blood. Lesions are visible as hypointense (dark) areas compared to white

matter. In ischemic damage increases in T_1, T_2 and proton density are connected to water accumulation due to vasogenic edema. T_1 and T_2 have been shown to correlate well with tissue water content in the gerbil brain and rat brain during ischemia (Kato et al., 1986).

2.2.3 Rotating frame, $T_{1\rho}$ and $T_{2\rho}$

$T_{1\rho}$ (T_1 rho) refers to the longitudinal relaxation (T_1) in rotating frame as it approximates T_1 in a very low magnetic field. The theory behind $T_{1\rho}$ relaxation was introduced in 1966 (Jones, 1966) and the first MR images were acquired in 1985 (Sepponen et al., 1985). The idea was to look at the decay of magnetization during a "spin lock" (SL) RF field and to achieve sensitivity to slow correlation times (τ_c).

In the on-resonance continuous wave (CW) SL technique (Sepponen et al., 1985) a 90° pulse is first applied to flip the magnetization, M_0, to the *xy*-plane. Then a low intensity RF locking field ($B_{1,SL}$) parallel to the M_0 is applied to keep the spins aligned with the effective magnetic field B_{eff} (during on-resonance SL $B_{eff} = B_{1,SL}$). In order for the spins to stay aligned in the locking field $B_{1,SL}$ must be higher than the local fields of water nuclei (the spin lock condition) (Abragam, 1961; Garwood and DelaBarre, 2001; Sepponen et al., 1985). The spin locked magnetization then rotates about the $B_{1,SL}$ in resonance condition with a precession frequency

$$\omega_{1,SL} = \gamma B_{1,SL} \quad . \tag{18}$$

While in the spin-lock the magnetization relaxes along the $B_{1,SL}$, with a relaxation time $T_{1\rho}$. Due to the low amplitude of the $B_{1,SL}$ field the resonance frequency ω_1 is low and therefore sensitive to slow molecular motions of the macromolecules. Furthermore, as $B_{1,SL}$ approaches zero, $T_{1\rho}$ approaches T_2 relaxation (Santyr et al., 1988). The $T_{1\rho}$ relaxation time constant can be defined as

$$\frac{1}{T_{1\rho}} = K_1\left(\frac{3}{2}\frac{\tau_c}{1+4\omega_{eff}^2\tau_c^2} + \frac{5}{2}\frac{\tau_c}{1+\omega_0^2\tau_c^2} + \frac{\tau_c}{1+4\omega_0^2\tau_c^2}\right), \tag{19}$$

where in case of on-resonance spin-lock the ω_{eff} is the frequency of the SL field i.e. $\gamma B_{1,SL}$ (Jones, 1966). In the slow molecular motion regime (large τ_c) the first term in equation (19) dominates and $T_{1\rho}$ is sensitive to processes that fulfill the condition $\omega_{eff} = 1/\tau_c$. The measured $T_{1\rho}$ relaxation decay follows equation (20)

$$M_t = M_0 e^{-T_{SL}/T_{1\rho}}, \tag{20}$$

where T_{SL} is the SL locking pulse duration. By changing the T_{SL} in successive images, quantitative absolute $T_{1\rho}$ images or maps can be calculated.

The effective SL field frequency ω_{eff} depends on both the on-resonance component $\omega_{1,SL}$ and the off-resonance component $\Delta\omega$ of the RF pulse:

$$\omega_{eff} = \sqrt{\omega_{1,SL}^2 + (\Delta\omega)^2}\,. \tag{21}$$

The off resonance SL technique gives the opportunity to lower the applied RF power (Santyr et al., 1994). By increasing the off-resonance frequency ($\Delta\omega$) higher B_{eff} can be achieved with the same B_1, as for the effective RF field B_{eff}

$$B_{eff} = \sqrt{B_1^2 + \left(\frac{\Delta\omega}{\gamma}\right)^2}\,. \tag{22}$$

Then the angle θ between B_{eff} and the transverse plane is

$$\theta = \tan^{-1}\left(\frac{\gamma B_1}{\Delta\omega}\right). \tag{23}$$

During the off-resonance the SL field, magnetization relaxes along the B_{eff}. The off-resonance $T_{1\rho}$ resembles the magnetization transfer (MT) experiment (see chapter 2.2.7), where an off-resonance pulse is used to saturate the bound water pool. Here the RF pulse is closer to the water peak than in MT (Ulmer et al., 1996), yet there is an effect of MT on the relaxation times. Also, there is an increasing effect of T_1 as θ increases (Gröhn et al., 2003; Henkelman et al., 2001). The off-resonance can also be used to sensitize $T_{1\rho}$ to different molecular motion regimes (Michaeli et al., 2004).

During adiabatic RF pulses the magnetization M_0 follows the effective rotating magnetic field B_{eff}, i.e. is under the spin-lock condition. Its orientation is time-dependent and a function of the amplitude and frequency modulations of the adiabatic full passage (AFP) 180° pulse. Also, with adiabatic pulses, such as the commonly used hyperbolic secant (HS) pulses, the contribution of slow molecular motion can be assessed (Michaeli et al., 2005; Michaeli et al., 2006). Relaxation rates can be altered by using different modulation functions. By changing the "stretching factor" n of the original HS (i.e. HS1) pulse the amplitude ω_1 (rad/s) and the orientation of the B_{eff} can be modulated. For HSn pulses

$$\omega_1(\tau) = \omega_1^{\max} \sec h(\beta\tau^n), \tag{24}$$

where β is a real constant governing the temporal width of the pulse (Garwood and DelaBarre, 2001; Silver et al., 1984).

With long SL pulses there is high power deposition into the target. This limits clinical use of SL MRI techniques due to the specific absorption rate (SAR) regulations. SAR measures the energy absorption from the applied RF power to tissue. It depends both on B_0 and B_1

$$SAR \propto (B_0 * B_{SL})T_{SL}/TR\,. \tag{25}$$

There are the United States' Food and Drug Administration (FDA) and the International Electrotechnical Commission (ICA) guidelines for SAR stipulating that less than 8 W of energy can be deposited for any kilogram in human body within an averaging time of six minutes. For the head there is a limit of 3.2 W/kg averaged over the head. There are $T_{1\rho}$ techniques to lower the SAR, for

instance by applying the full power spin-lock pulse to the central phase-encode lines of the k-space only (Wheaton et al., 2004). Also, by using adiabatic (HS*n*) pulses this deposited energy can be lowered (**III**).

There are several relaxation processes effective at low field that can give specific information about water-macromolecule interactions (Borcard, 1984). The sensitivity of $T_{1\rho}$ to molecular fluctuations at the kHz range makes it a good tool to study dipolar interactions, water dynamics and interactions with endogenous macromolecules (Liepinsh and Otting, 1996). Furthermore, sensitivity of $T_{1\rho}$ relaxation to alterations in molecular weight, concentration and structure of proteins and chemical exchange (Mäkelä et al., 2001; Virta et al., 1997) makes it sensitive to early events in stroke (Gröhn et al., 1999; Gröhn et al., 2000a; Kettunen et al., 2001) as well as an MRI indicator of tissue damage. $T_{1\rho}$ provides a good inherent contrast between different brain structures (Borthakur et al., 2004) and has been used for structural imaging of the human brain (Gröhn et al., 2005; Michaeli et al., 2006; Ramadan et al., 1998; Wheaton et al., 2004). Furthermore, the on-resonance $T_{1\rho}$ has been shown to be a more sensitive tool to detect acute ischemia than the off-resonace $T_{1\rho}$ (Gröhn et al., 2003). $T_{1\rho}$ MRI reveals ischemia earlier than diffusion MRI does (Kettunen et al., 2001).

$T_{1\rho}$ contrast has recently been used in the imaging of various tissues and animal models for human diseases (including brain infarct (Sepponen et al., 1986), Alzheimer's disease (Borthakur et al., 2008; Haris et al., 2009), breast cancer (Santyr et al., 1989), head and neck tumors (Markkola et al., 1998), cartilage (Regatte et al., 2003), muscle (Lamminen et al., 1993; Virta et al., 1998), etc.). While still under investigation, $T_{1\rho}$ MRI is being transferred to clinical use owing to its good potential in several disease models.

During adiabatic rotation magnetization M follows $\omega_{\text{eff}}(t)$, which is time dependent. In the ω_{eff} frame (tilted doubly rotating frame, x´´y´´z´´) the components that are aligned with M (and ω_{eff} and $z´$) will relax with the time constant $T_{1\rho}$, whereas the components perpendicular to M (on the $x´´y´´$ plane) will relax with the time constant $T_{2\rho}$ (Michaeli et al., 2004). Thus the adiabatic rotating frame relaxation time, $T_{2\rho}$, describes the relaxation of the magnetization that is perpendicular to the effective magnetic field B_{eff}. $T_{2\rho}$ relaxation takes place during the adiabatic Carr-Purcell spin echo sequence with zero interpulse delays. It is a function of dipolar interactions and affected by the proton exchange. The $T_{2\rho}$ relaxation time constant due to dipolar interactions can be defined as

$$\frac{1}{T_{2\rho}} = K_2\left(3\tau_c + \frac{3\tau_c}{1+4\omega_{eff}^2\tau_c^2} + \frac{14\tau_c}{1+\omega_0^2\tau_c^2} + \frac{20\tau_c}{1+4\omega_0^2\tau_c^2}\right). \quad (26)$$

As the adiabatic rotating frame relaxation time constants depend on the modulation function, also $T_{2\rho}$ relaxation rate can be altered by changing the modulation function. $T_{2\rho}$ can be measured using the rotary echo technique (Solomon, 1959) or with AFP pulses using, for instance, the HS*n* type pulses (Michaeli et al., 2004).

2.2.4 Blood Oxygenation Level-Dependent MRI

Brain activation causes changes in the oxyhemoglobin-to-deoxyhemoglobin ratio. The oxyhemoglobin is diamagnetic and deoxyhemoglobin paramagnetic. T_2 relaxation of blood is strongly determined by the hemoglobin oxygenation level and hematocrit, factors that constitute the basis for blood oxygenation level dependent (BOLD) contrast (Ogawa et al., 1990). This provides endogenous contrast for functional MRI (fMRI), because brain activation is associated with decreased susceptibility difference between blood and tissue. Both T_2 and T_2* MRI can be used for readout of the BOLD contrast. T_2* has higher sensitivity than T_2 to BOLD, but due to contributions of nonspecific magnetic field inhomogeneities and susceptibility differences at tissue interfaces to T_2*, use of this fMRI technique for quantification of physiological factors is more difficult (Roussel et al., 1995).

BOLD contrast is sensitive to changes in blood oxygenation and can be used to assess deoxygenation or reoxygenation in ischemia and reperfusion by imaging the mismatch between oxygen delivery and consumption (De Crespigny et al., 1992). It can be a tool in assessing tissue in risk and tissue viability in acute stroke (Gröhn and Kauppinen, 2001). Furthermore, BOLD MRI can be used to assess the cerebrovascular reserve (Kleinschmidt et al., 1994), tissue metabolism and the "residual oxidative activity" (Gröhn and Kauppinen, 2001; Gröhn et al., 2000b; Lythgoe et al., 2000). Most often BOLD contrast has been exploited in fMRI (Belliveau et al., 1991; Moonen et al., 1990).

2.2.5 Diffusion MRI

Diffusion is an expression of random (Brownian) motion of water molecules in tissue. Molecules can randomly change their position and orientation. This leads to time dependent displacement of the molecules. According to Stokes-Einstein relation in an isotropic material the diffusion constant D is defined as

$$D = \frac{k_B T}{6\pi\eta R_H}, \tag{27}$$

where k_B is the Boltzmann constant, T is the absolute temperature, η is the viscosity of the medium and R_H is the hydrodynamic radius, i.e. the radius of a sphere that diffuses with the same rate as the molecule. In tissue the diffusing particles are affected by cellular membranes and other barriers inside and outside of the cell, different transport processes and interaction with macromolecules. In MRI the diffusion in tissue is often described with the apparent diffusion coefficient (ADC). This

takes into account also the permeability of membranes and the binding to macromolecules. It can be written as

$$ADC = D/\lambda^2 , \tag{28}$$

where D is the self diffusion coefficient and λ the tortuosity coefficient describing the diffusional path length between two points.

In diffusion MRI strong magnetic field gradients are incorporated, for example into a spin echo sequence. These will render the MRI pulse sequence sensitive to the displacement of the water molecules. The displacements are restricted by cell structures (fibers and membranes) and transport processes and thus they are different in different directions. The ordinary diffusion MRI is based on the Stejskal-Tanner pulse sequence (Stejskal and Tanner, 1965), in which a gradient pulse is applied on either side of the 180° refocusing pulse with gradient amplitude G and duration δ separated by time Δ. The first pulse causes the spins to dephase. If there is no displacement during the diffusion time, the second gradient pulse will nullify the phase change resulting in zero loss of magnetization. If there is displacement the rephasing will be incomplete attenuating the MR signal. The diffusion weighting factor b can be defined as

$$b = \gamma^2 G^2 \delta^2 (\Delta - \delta/3) , \tag{29}$$

where γ is the gyromagnetic ratio of the nucleus. The decrease in signal intensity can be calculated from

$$S(b) = S_0 e^{-b \cdot D}, \tag{30}$$

where $S(b)$ is the signal intensity with diffusion weighting b and S_0 is the signal intensity at $b = 0$.

To take into account the orientation dependency of diffusion weighted imaging (DWI) contrast due to neuronal fibers or other oriented structures (Moseley et al., 1990) a diffusion tensor can be calculated. It provides information about the tissue fiber orientations and connectivity in the brain (Basser and Pierpaoli, 1996; Le Bihan et al., 2001; Mori et al., 1999). From this an orientation independent estimate of the diffusion constant D_{av} can be calculated (Mori and van Zijl, 1995; Moseley et al., 1990; van Gelderen et al., 1994; Wong et al., 1995)

$$D_{av} = \frac{1}{3} Trace\left\{\overline{\overline{D}}\right\} = \frac{1}{3}\left(D_{xx} + D_{yy} + D_{zz}\right), \tag{31}$$

where D_{xx} is the diagonal element of the diffusion tensor, where the pair of diffusion gradients is applied along the x-direction. By combining the data of different directions an image showing the average diffusion is acquired. In practice this data can be calculated by incorporating at least three orthogonal diffusion gradients (Basser et al., 1994a; Basser et al., 1994b) or by using combinations of two or three simultaneous bipolar diffusion gradients in three orientations in a single scan (Mori and van Zijl, 1995).

DWI is a sensitive way to reveal early acute ischemia in the brain. An area with restrictions in the water diffusion path appears brighter in the images. For quantitative diffusion values images taken with different diffusion weighting, i.e. multiple *b*-values, are needed. The ADC maps are obtained by fitting a mono-exponential function (Eq. 30) for each pixel of these images.

DWI can be used to monitor the evolution of the ischemic lesion from the hyperacute stage to the chronic stage. DWI signal enhancement is visible only when CBF falls below a certain threshold (about 20ml/100g/min for gerbils) (Busza et al., 1992), which is the threshold for normal cell metabolic homeostasis and depolarization (Allen et al., 1988; Crockard et al., 1987). The changes can be seen within 2 minutes from the onset of ischemia (Davis et al., 1994; van der Toorn et al., 1994). Increase of signal intensity within 15 minutes in DWI was first shown in the ischemic cat brain (Moseley et al., 1990), demonstrating decrease in the diffusivity of water. In human stroke, DWI signal intensity has been shown to increase during the first 3-4 days after ischemia and then to slowly decrease (Lansberg et al., 2001). ADC values return to normal by 2-3 days after the onset of ischemia in rats (Jiang et al., 1993) but this is followed by an increase in the diffusion after one week (Knight et al., 1994; Verheul et al., 1992). This is due to the cellular lysis (Pierpaoli et al., 1993), where structural destruction of cells and the increase of water cause an increase in the ADC values. There is a notable difference between the contrasts of ADC and DWI images in the hyperacute phase of ischemia. The DWI images may show the hyperintense lesion area due to the "shine through" effect of T_2. This is because the diffusion sequence is often also T_2 weighted and therefore the DWI is influenced by both T_2 weighted signal intensity and diffusion effects. The ADC map on the other hand shows just the diffusion effect.

The most common explanation for the reduction in the diffusion of water molecules (the ADC) in stroke is cytotoxic edema. However, several other explanations have been presented to account for the mechanisms underlying the ADC change, as described in chapter 2.1.3.

Clinical studies have shown the feasibility of the use of diffusion MRI in assessing human stroke (Warach et al., 1992). The irreversible injury to tissue occurs due to prolonged lack of energy and the lesion, as determined by ADC, correlates with histological damage (Jiang et al., 1993). Cytotoxic edema begins within minutes after ischemia, but if the ADC returns to normal shortly a reversible ischemic damage is possible. However, this depends on the duration of the ischemia and how much ADC has decreased.

2.2.6 Perfusion

CBF is intimately linked to ischemic stroke; ischemia results from insufficient blood flow. Along with diffusion MRI, revelation of perfusion by MRI is a key parameter in characterizing hemodynamics during ischemic stroke. Perfusion MRI allows direct assessment of blood delivery into capillary bed of tissue at any given time following the onset of ischemia. Perfusion takes place at the capillary level and it is related to the delivery of oxygen to the tissue. Perfusion MRI has the potential to indicate the level of risk of a region to develop ischemic damage. Measuring CBF in absolute terms will give a handle on the degree of compromised perfusion, and indirectly, this may indicate potentially salvageable tissue.

CBF measures the flow of blood that is delivered to a tissue. Typical CBF for human gray matter is around 60 ml/100g of tissue per minute (white matter about 20-25 ml/100g/min) and for rats approximately 120 ml/100g/min. Astrup et al. showed two CBF thresholds found in the ischemic core and the surrounding penumbra that differentiate the area between electrical failure and the release of K^+ that leads to cell death (Astrup et al., 1977). Interestingly, there is a difference in the lesion size as revealed by diffusion and perfusion in the acute phase. This diffusion-perfusion mismatch is often linked with the ischemic penumbra, but recent evidence shows that that is not always the case (Sobesky et al., 2005).

2.2.6.1 Dynamic susceptibility contrast enhanced MRI

A routine technique to determine cerebral perfusion has been the dynamic susceptibility contrast enhanced (DSC) MRI or bolus tracking, where an injection of a paramagnetic contrast agent, such as gadolinium(III)-diethyltriaminepentaacetic acid (Gd-DTPA), is given intravenously as a quick bolus into a peripheral vein (Belliveau et al., 1990; Rosen et al., 1990). This contrast agent causes changes in the local magnetic field shortening of T_2* relaxation time in target organ. After the injection rapid acquisition of T_2* weighted MR data is performed, as the first passage of the bolus lasts only a few seconds. The transient signal loss due to dephasing (shortening of T_2*) (Villringer et al., 1988) is then recorded as a time intensity curve.

Not only CBF but several other parameters can be measured from the time intensity curve of DSC MRI relevant to the pathophysiology of acute stroke. Time to peak (TTP) is the time from injection of the contrast agent to maximum signal drop in the image. Mean transit time (MTT) is time between the arterial inflow and the venous outflow of blood, i.e. the average time for an injected bolus to pass through tissue. Cerebral blood volume (CBV) is the volume of blood per unit of brain mass. Estimation of the CBF can be made with the central volume theorem

$$CBF = CBV/MTT\ . \tag{32}$$

MTT and TTP are good indicators for hemodynamic impairment, whereas CBF is a better one for predicting ischemic lesion outcome (Parsons et al., 2001; Rivers et al., 2006). It should be noted that CBV does not differentiate between irreversibly damaged and recovering tissue, however, (Rohl et al., 2001) and DSC MRI gives only semi-quantitative information about the perfusion of the tissue, normal or ischemic. For reliable results for the parameters above clearance of contrast agent should also be taken into account as well as a defined bolus.

DSC is the clinically most often used MRI method for perfusion imaging, due to its high contrast to noise ratio (CNR). Gradient echo (GRE, FLASH) or echo-planar imaging (EPI) MRI sequences are used as fast imaging techniques for DSC MRI. Also dynamic contrast enhanced (DCE) imaging exploiting changes in T_1 may be used to study tissue vascularity and permeability. It has been mainly used for cancer applications, including assessment of angiogenesis in tumors (Barrett et al., 2007). In DCE a different time scale is used as the imaging time is between 5 and 10 minutes, thus not just the first pass of the bolus is observed.

2.2.6.2 Arterial spin labeling

Arterial spin labeling (ASL) is an MRI technique to quantitatively study the cerebral perfusion, mainly CBF. In ASL water protons in blood are labeled with RF-pulses and thus, no external contrast agent is needed. The magnetization of the arterial blood is typically inverted or saturated with a spatially selective RF pulse, or a pulse train, before it enters the perfused tissue of interest. With the flow of blood the labeled protons migrate to tissue and exchange with the extravascular water thus affecting the characteristic magnetization and relaxation of the tissue water (Detre et al., 1992; Williams et al., 1992). Following tagging after an inversion time (TI) a spin-labeled image is acquired of the region of interest (ROI). A control image is then acquired usually by tagging an area symmetrically on the other side of the imaged area, e.g. outside the head, to account for MT contribution in the blood flow image. Assuming there are equal signals from static spins in both images, the tagged image is subtracted from the control image. The difference image then reflects the amount of blood that has flowed into the ROI during the time TI in exchange at capillary site with tissue and thus, the signal is directly proportional to CBF. Different tagging schemes have been used with different control pulses and their variations as reviewed by Wong et al (Wong, 2005).

Quantification of absolute CBF by ASL is possible if inversion (labeling) efficiency, tissue T_1 and tissue-water ratio are known (Calamante et al., 1999b; Thomas et al., 2000). Efficient inversion is needed for good contrast. A bolus of tagged blood with well defined temporal width is needed and it should be fully delivered to the target tissue (Alsop and Detre, 1996; Wong et al., 1998).

Furthermore, decrease in the magnitude of the magnetization tag caused by relaxation needs to be taken into account. In ASL, spin-labeled blood is used as an endogenous contrast media, in comparison to DSC that uses external contrast tracers. Therefore in ASL the tag can only last about the time of T_1 of blood, i.e. roughly 1-1.5 seconds. Thus the labeling time must be longer than that. Further, a spatial gap is needed to take into account the imperfections in the spatial labeling pulses. This causes a transit delay (Δt) between the tagging of the blood and the blood delivery to the ROI. This delay needs to be minimized for accurate quantification.

Two types of techniques can be used for MR labeling, continuous and pulsed ASL. In the original technique of continuous arterial spin labeling (CASL) (Detre et al., 1992; Williams et al., 1992) blood flowing into the brain is continuously inverted at the neck level. With a single long, low-power RF pulse of several seconds and a magnetic field gradient, a steady state of brain tissue magnetization is generated. The CASL technique relies on the flow-induced adiabatic inversion.

In pulsed arterial spin labeling (PASL) a single RF-pulse or a train of pulses close to the region of interest is used to tag the arterial blood. HS pulses or similar adiabatic pulses are often used to achieve efficient inversion (Williams et al., 1992). These are also relatively insensitive to B_1 inhomogeneity and resonance offsets. Different pulses have been introduced to improve the tagging slice profile (Frank et al., 1997; Yongbi et al., 1998). Still, with PASL tagging efficiency is often above 95% (Wong et al., 1998). Newer labeling techniques include the velocity selective ASL (VS-ASL), where blood is tagged, i.e. saturated or inverted, based on the velocity not location (Duhamel et al., 2003). Here only spins that decelerate through a cutoff velocity during TI will be observed.

2.2.6.3 Magnetic resonance angiography

A technique for imaging cerebral blood vessels using MR is magnetic resonance angiography (MRA), where the large vessels can be visualized along with quantification of the blood flow. It can be used to locate abnormalities such as stenoses and occlusions in stroke patients and to estimate perfusion in the brain. Similar to ASL MRI no exogenous contrast medium is necessary. MRA contrast can be achieved with repetitive RF pulses that saturate tissue and thus enhance flow related contrast. Two basic MRA techniques are time-of-flight (TOF), where the spins that are moving into the imaging slice appear brighter than the surrounding tissue (phase difference) and phase contrast MRA (PC-MRA), where the correlation between the phase of the moving spins and the velocity of the blood flow (phase dispersion) is exploited. The problem with MRA is the low spatial in-plane resolution. Contrast enhanced MRA (CE-MRA), involving intravenous injection of Gd-based contrast agent, is used clinically to achieve higher spatial resolution (Anzalone, 2005).

MRA can be clinically used for studying arteries in the head and neck in patients at risk of stroke. It is non-invasive, as there are no catheters introduced in the body. It has also been used to study cerebral vasculature in stroke patients (Barber et al., 1999; Edelman et al., 1990; Rordorf et al., 1998; Schomer et al., 1994).

2.2.7 Magnetization transfer and Z-spectroscopy

MT imaging takes advantage of the interaction between free water pool and the semi-solid macromolecule pool (Wolff and Balaban, 1989). The two pools of water in tissue create two peaks in the MR spectrum (Balaban and Ceckler, 1992). Under the narrow bulk water peak resides a broad macromolecule resonance peak caused by largely varying resonance frequencies within macromolecules. By saturating the macromolecular pool either with a low power RF irradiation or pulsed saturation centered away from the bulk water peak, reduction in the free water signal is observed. Due to the exchange of magnetization between the two pools the applied off-resonance B_2 field results in signal loss of the free water. The MT effect is described by the magnetic transfer ratio (MTR) that can be written as

$$MTR = 1 - \frac{M_{sat}}{M_0}, \tag{33}$$

where M_{sat} is the saturated magnetization and M_0 the steady state magnetization.

Plotting the MTR amplitude as a function of the frequency offset of the saturating RF-pulse (B_2) produces the Z-spectrum (Bryant, 1996). The Z-spectrum associated with macromolecules in tissue is slightly asymmetric around the free water resonance peak (Pekar et al., 1996). This MT asymmetry is considered to be due to chemical shift center mismatch between the free water and macromolecules in tissue. This asymmetry significantly affects the CASL experiments for quantification of CBF.

MRI exploiting the MT contrast (Ordidge et al., 1991) showed reduction in magnetization exchange rate between bulk and bound water protons peaking at 24h in a rat model of cerebral ischemia. This may be related to the increased amount of interstitial water caused by vasogenic edema (Ewing et al., 1999; Mäkelä et al., 2002). MT contrast comes mainly from the dipole-dipole interaction between the two water pools. *In vivo* MT mostly consists of cross-relaxation via molecular exchange pathways, but proton exchange may also have a contribution (Grad et al., 1991; Wolff and Balaban, 1989). The rate of MT gives information about the ratio between bound and free water pools in tissue. With a two pool model of exchange the relaxation characteristics of the pools can be assessed (Henkelman et al., 1993; Henkelman et al., 2001).

Effects of MT in MR images can be revealed by a continuous RF pulse (continuous wave, CW) or by short RF pulses (pulsed MT). MT contrast can be used to improve MRA and the MT effect can give valuable information about mechanisms contributing to it. It can also cause an unwanted contrast change in MR imaging, for instance when the RF pulses are applied in short succession (Dixon et al., 1990) and in some imaging sequences, such as FSE (Constable et al., 1992).

2.2.8 Amide Proton Transfer Ratio and pH

Amide proton transfer (APT) exploits an MT pathway, where the contrast is produced by the change in water resonance peak due to chemical exchange. The amide proton resonance peak resonates at 3.5 ppm (parts per million) downfield from water resonance peak (Mori et al., 1998; van Zijl et al., 2003; Zhou et al., 2003b). APT contrast reflects the relative changes in pH, the amount of exchangeable amide protons of proteins/polypeptides and water content (Zhou et al., 2003b).

The amide proton transfer ratio (APTR) can be measured as MT ratio (MTR) asymmetry of the Z-spectrum at ±3.5 ppm from the water peak (Zhou et al., 2003b):

$$APTR = MTR(-3.5\,ppm) - MTR(3.5\,ppm) = \frac{S_{sat}(-3.5\,ppm)}{S_0} - \frac{S_{sat}(3.5\,ppm)}{S_0}, \qquad (34)$$

where S_{sat} and S_0 are the saturated and unsaturated signal intensities respectively. Asymmetry in Z-spectra in the amide group region has been shown to change during acute ischemia (Sun et al., 2007b; Zhou et al., 2003b). This change can be seen as the difference in APTR (ΔAPTR) between the ischemic (ipsilateral) and the normal (contralateral) sides of the brain. As the proton exhange rate is proportional to the change in pH (Englander et al., 1972; Liepinsh and Otting, 1996), APTR has been proposed a means to image intracellular pH changes in the brain (Zhou et al., 2003b). The small asymmetry of the macromolecule associated Z-spectrum also causes a non-zero background in the asymmetry plot in the amide proton transfer (APT) analysis.

2.2.9 Magnetic Resonance Spectroscopy

The electron cloud surrounding the nucleus has a shielding effect against the external magnetic field and causes an additional field that changes the effective field sensed by the nucleus. The “chemical environment” causes the nucleus to resonate at a slightly different Larmor frequency. The shielding effect on nuclear resonance frequency is called the chemical shift. Due to different chemical shifts, there are several frequencies in the MR spectrum from multiple spin systems with different resonant

frequencies. This information gives a tool to identify and quantify metabolite resonances by MR spectroscopy (MRS). Several resonance peaks can be identified such as N-acetyl aspartate (NAA), total creatine, choline containing compounds, glutamate and glutamine, myo-inositol and taurine and lactate. Acute cerebral ischemia is associated with both increase and decrease of many of these peaks (Hoehn et al., 2001). Despite the rather low sensitivity, MRS can be used *in vivo* to detect non-invasively metabolites that have high (mM) concentration.

The most prominent ^{1}H MRS marker in the brain is NAA. It is often used as a marker of neuronal density in mature brain and its concentration decreases in ischemic stroke due to neuronal damage and dysfunction. Quantification can be done using the ratio of one metabolite to one that has a known constant quantity. Often creatine is used as an internal standard as it is relatively resistant to change in the hyperacute phase of ischemia and has constant concentration throughout the brain (Howe et al., 1993). Another good early 1H MRS marker of ischemia is lactate (Schurr, 2002; Siesjö and Nilsson, 1971) that is produced by anaerobic glycolysis. In infarcted tissue elevated lactate levels and diminished levels of NAA are usually observed (Graham et al., 1995). In acute infarct a small change in the choline level can also be seen, and there are studies showing a drop in total creatine during ischemia (Berkelbach van der Sprenkel et al., 1988; van der Toorn et al., 1994).

Apart from proton (^{1}H) MRS, phosphorus (^{31}P) MRS has been used for brain studies owing to its sensitivity to ischemia and the lack of need for water and fat suppression. ^{31}P MRS can detect the loss of high energy phosphates in acute cerebral ischemia (Welch et al., 1992; Williams et al., 1989) and measure the intracellular pH (pH_i) from the chemical shift of inorganic phosphate. Decrease in pH_i is strongly associated with intracellular lactate concentration (Combs et al., 1990). Some other nuclei have been used in metabolic MRS studies of ischemia, such as ^{13}C and ^{23}Na as reviewed by Kauppinen and Williams (Kauppinen and Williams, 1994; Williams et al., 1989).

2.2.10 Multiparametric MRI

Confirming the presence of ischemia in the brain is achieved with a single MRI contrast (e.g. diffusion MRI), but prediction of the final lesion size is still a challenging goal for stroke MRI. A single MRI parameter or a time series can hardly describe the complex nature of events associated with evolution of ischemic damage. A combination of multiple MRI parameters is required for an evaluation of the pathological state of tissue. Multiparametric MRI is expected to allow a more accurate assessment of the evolution of an ischemic lesion. In short: T_2 weighted imaged with ADC data can separate between acute and chronic lesions, areas showing perfusion deficiency without DWI lesion can predict damage progression, MRA provides data from blood flow in large vessels,

DSC perfusion MR imaging shows blood flow delays in the capillaries and BBB breakdown and T_2* weighted MRI assess the possible hemorrhage. In the clinical setting several MRI parameters can routinely be measured during one imaging session within a tolerable time.

The mismatch between the lesion size projected by perfusion and diffusion weighted images has long been the basis in predicting lesion growth during ischemia, i.e. the diffusion-perfusion mismatch (Warach et al., 1996). Welch et al. used T_2 and ADC values to assess the degree of ischemic damage in rats (Welch et al., 1995). Several other MRI parameter combinations have also been used to study the evolution of cerebral stroke (Carano et al., 2000; Carano et al., 1998; Jacobs et al., 2000; Mitsias et al., 2002; Welch et al., 1995; Wu et al., 2001). The Iterative Self-organizing Data Analysis Technique Algorithm (ISODATA) is one widely used technique for an unsupervised computer segmentation of lesion during ischemic stroke (Jacobs et al., 2000; Soltanian-Zadeh et al., 2003). It has also been used to predict tissue fate (Shen et al., 2004; Shen et al., 2005) and the final lesion size (Lu et al., 2005). Lately, multiparametric MRI has been used to study new treatment methods for stroke (Ding et al., 2004; Li et al., 2005; Li et al., 2007; Li et al., 2006). These studies argue for complementary aspect of various MRI contrasts to obtain more comprehensive image of tissue status in ischemia from single time point examination. Furthermore, multiparametric MRI has the potential for both diagnostic and prognostic value for both clinical and experimental studies and routine patient imaging.

3 AIMS OF THE STUDY

The aim of this PhD research project was to characterize dynamic changes in MRI parameters in ischemic brain tissue, with a special reference to alterations in water spin dynamics and apply multiparametric MRI for predicting the time-dependent progress of ischemia. To these ends *in vivo* stroke studies were performed to measure several established and novel MRI parameters at several time points during (hyper-)acute ischemia in a permanent MCA occlusion model, after a temporary MCAo with reperfusion and after a photochemically induced permanent cortical stroke model.

The specific aims for these studies were the following:

- to examine the interrelationship between APTR and pH_i derived from tissue lactate during focal cerebral ischemia in rat (**I**)
- to study the temporal interrelationship between diffusion, $T_{1\rho}$ and APTR during and after the ischemic insult (**I**)
- assess the evolution of brain pathology including hemorrhage by MRI in rats with a photochemically induced cortical infarct in relation to sensorimotor impairment (**II**)
- to investigate the abilities of various $T_{1\rho}$ and $T_{2\rho}$ MR approaches with inherently differing SARs to reveal hyperacute ischemia (**III**)
- to evaluate alterations in water spin dynamics during evolving cerebral ischemia using the MR relaxation data in the context of an equilibrium two-site exchange (2SX) model (**III**)
- to investigate the correlation between different combined MRI contrasts and quantitative cell damage (**IV**)

4 MATERIALS AND METHODS

4.1 Animals

Male Wistar rats weighing 280-330 g were used in these studies. The studies were conducted according to guidelines set by the Council of Europe (Directive 86/609) and approved by the ethical committee of the National Laboratory Animal Center at the University of Kuopio.

During the experiments the rats were monitored to keep the physiology as close to normal as possible. Core temperature was monitored online and a plastic heating pad with circulating water was placed under the rat. Blood pressure was monitored (**I**, **III**) online with an arterial catheter system (CardioCap II, Datex, Helsinki, Finland) and arterial blood gases (pCO_2, pO_2) were checked (**I**, **III**, **IV**) by blood samples taken just before the first MRI scan and after 1 hour between scans (i-Stat Co., East Windsor, NJ, USA). Breathing was monitored (**IV**) online (SA Instruments, Inc, Stony Brook, NY, USA).

4.1.1 Anesthesia and analgesia

Anesthesia was maintained during the surgery and imaging by 1.5% halothane (**I**, **II**) or isoflurane (**III**, **IV**) mixed with a continuous flow of 70%/30% N_2O and O_2. Animals were breathing freely through a face mask. For long MRI studies (over 1 hour per animal inside the scanner) arterial blood pressure (**I**, **III**) or breathing rate (**IV**) was monitored during the MRI to control the depth of the anesthesia. Saline injection was given intra-peritoneally before imaging to prevent dehydration during imaging. For post-operative pain Rimadyl (carprofen, 0.1ml/100g, Pfizer) was injected sub-cutaneously as an analgesic in study **IV** after the first day of imaging. After the study the animals were sacrificed with an overdose of halothane or isoflurane (**I**, **III**) followed by cervical dislocation (**I**, **III**). In studies **II** and **IV** the animals were perfused under deep anesthesia for histology.

4.1.2 Ischemia

Cerebral ischemia was induced in rats by MCA occlusion (**I**, **III**, **IV**) (Longa et al., 1989). Through a cervical incision a nylon thread (diameter 0.22 mm) was inserted via the external carotid artery (ECA) through the internal carotid artery (ICA) until it reached the origin of the MCA to block the

blood supply. Reperfusion (deocclusion) was performed by retracting the thread 6-8 mm after 60 (**IV**) or 90 (**I**, **III**) minutes from the onset of ischemia to enable spontaneous reperfusion. In study **II** a photochemically induced permanent cortical infarct was used with Rose Bengal dye (Sigma) that induced a consistent and precise infarct lesion. Light activation of the dye causes free radical formation and endothelial cell damage. This leads to aggregation of platelets and further to the occlusion of the blood vessel.

4.1.3 Limb-placing test

In study **II** a limb-placing test was performed to assess the sensorimotor integration of fore limb and hind limb responses to stimulation before and after ischemia. The tests were performed on both the left and the right side to address the impairment and the recovery.

4.1.4 Histology

In studies **II** and **IV** histological analysis was performed. In study **II** the rats were first anesthetized and then the brains were perfused. 50 μm slices were cut with a microtome and then stored in a cryoprotective solution in -20 °C. The sections were stained with Perl's Prussian blue to locate hemorrhage by ferric ion (Fe^{3+}) deposits. In study **IV** after PFA perfusion the brains were cryoprotected and later sliced to 30 μm slices for staining. Cresyl violet staining was used for cell counting to locate viable cells in the regions of interest. The stained slices were visually correlated to the MRI slices with the help of Paxinos rat brain atlas (Paxinos and Watson, 1996).

4.2 NMR/MRI Methods

4.2.1 Hardware

A Magnex 4.7 T horizontal bore scanner (Magnex Scientific Ltd., Abingdon, UK) with a Varian Inova interface (Varian, Palo Alto, CA, USA) was used for MR imaging and spectroscopy. A quadrature surface coil (loop diameter 20 mm) with transmit/receive mode (HF Imaging LLC, Minneapolis, MN, USA) (**I**, **II**, **III**) or a Rapid quadrature coil with a volume transmitter and actively decoupled quadrature surface coil receiver (Rapid Biomedical GmbH, Rimpar, Germany)

(**IV**) were used for imaging. An in house built animal holder (animal in supine position) was used for animal setup to accommodate the retraction of the occluder in MCAo studies of temporary ischemia.

4.2.2 Data acquisition

A line scanning method was used in study **I**. The imaging line (3 mm x 3 mm x 35 mm, 128 pixels along the line) was positioned 4 mm caudally from the olfactory bulb and 4 mm from the surface of the brain going through striatum and the parietal cortex. Mean values of the data for ipsi- and contralateral striatum were calculated. For the rest of the studies (**II**, **III**, **IV**) 2D images were acquired. Most of the imaging sequences were done with fast spin echo (FSE) readout. Only the average diffusion was measured with spin echo (SE) readout. Scans were acquired with sets of several MRI parameters (e.g. T_1, T_2, $T_{1\rho}$ and $T_{2\rho}$ with continuous wave or with HS*n* pulses, diffusion, perfusion (ASL) and MT/APTR sequences). Maps of the corresponding parameters (e.g. T_1, T_2, $T_{1\rho}$, D_{av}, etc) were then calculated accordingly.

In the 2D studies the image matrix size was set to 256 x 128 (**II**) and for all parameter maps 128 x 64 (**II**, **IV**) except in (**IV**) 64 x 32 for perfusion and APTR. The field of view (FOV) was set to 2.56 cm x 2.56 cm (**III**, **IV**), 35 mm x 35 mm (**II**). Slice thicknesses were 1 mm (**II**) or 1.5 mm (**III**, **IV**). The imaging plane was positioned 5 mm caudally from the olfactory bulb (**IV**) or 4 mm from the surface of the brain (**III**). In study **II** a 3D stack of 12-14 slices covering the whole lesion volume was acquired.

As a quality check the variations in the B_1 field were measured (**I**, **III**, **IV**) by using a variable length square preparation pulse with FLASH readout (TR = 4.5 ms, TE = 2.2 ms). A cosine function was then fitted to the signal intensity oscillation to calculate the field strength.

4.2.3 T_1 and T_2

T_1 was quantified in study **IV**. An inversion recovery sequence with five inversion times (TI = 5 - 1500 ms, TR = 3 s) was used with FSE readout sequence.

For T_2 weighted images and T_2 maps (**II**) a multislice acquisition using a double SE sequence with adiabatic refocusing was used (TR = 3 s, TE = 80 ms and TE = 15, 40, 65 ms, TR = 1.5 s, respectively). In studies **III** and **IV** the T_2 maps were collected using a preparation block consisting

of an adiabatic AHP-TE/4-AFP-TE/2-AFP-TE/4-reverse AHP sequence followed by fast spin echo (FSE) readout sequence.

T_2* weighted images were measured in study **II** to assess the hemorrhagic area. A standard gradient echo (GE) imaging sequence was used (TE = 15 ms, TR = 700 ms, flip angle 50°).

4.2.4 $T_{1\rho}$ and $T_{2\rho}$

For conventional on-resonance CW-type $T_{1\rho}$ imaging adiabatic half passage (AHP) pulses were used before and after the spin-locking pulse. (See study **III** Figure 1 for a schematic illustration of the preparation pulse sequences.) The $T_{1\rho}$ linescan data in study **I** were measured using adiabatic spin-lock pulses with five different spin-lock times (T_{SL} = 10 - 90 ms, $B_{1,SL}$ = 0.6 G, γB_1 = 2550 Hz, TR = 2.5 s, TE = 15 ms). For 2D CW-type $T_{1\rho}$ (**III**, **IV**) spin-lock times from 8 to 64 ms and FSE readout (echo spacing 10 ms, 16 echoes, TR = 2.5 s, TE = 6 ms) were used with the locking field $B_{1,SL}$ = 0.8 G (**III**) and 0.4 G (**IV**). The CW-type $T_{2\rho}$ (**III**) data were acquired with a rotary echo technique (Solomon, 1959) with FSE readout.

For adiabatic $T_{1\rho}$ (**III**, **IV**) and $T_{2\rho}$ (**III**) hyperbolic secant (HS*n*) pulses were used (Garwood and DelaBarre, 2001; Silver et al., 1984). A train of 4 - 32 adiabatic full passages (AFPs) were used and the pulse phases prescribed according to MLEV-4 scheme (pulse duration 2 ms with no inter pulse delay).

4.2.5 Diffusion

Diffusion MRI was acquired in the studies **I**, **III** and **IV** to assess the severity of the ischemic insult. Quantitative average diffusion was acquired as trace of diffusion tensor maps. Four bipolar gradients along each axis with four b-values (0 - 1370 s/mm^2) (**I**, **III**, **IV**) were used with SE readout (TR = 2.5 s (**I**), or TR = 1.5 s (**III**, **IV**), TE = 55 ms) (Mori and van Zijl, 1995).

4.2.6 Perfusion, ASL

In study **IV** CBF was measured using a CASL technique, with a 3.0 s labeling pulse, 3.0 s and 500 ms pre and post labeling delays respectively. The labeling pulse was centered 2 cm caudally from the imaging plane. CBF was estimated from the formula

$$CBF = \Delta M * \lambda / 2T_1 , \quad (35)$$

where ΔM is the magnetization difference between the labeled and control images and λ the blood-brain partition coefficient. The average of eight label-control pairs was used for the calculations.

4.2.7 Amide proton transfer ratio and intracellular pH

In study **I** the Z-spectra were acquired by saturating the off-resonance frequencies with a train of 6.6 ms long 180° Gaussian pulses (γB_1 = 50 Hz) with an interpulse delay of 3.4 ms for 4 seconds. The 41 offset frequencies were located 0 - 2 kHz symmetrically around the water peak (TR = 7 s, TE = 15 ms). Changes between the ipsi- and contralateral side in the APTR (ΔAPTR) were calculated from the asymmetry in the Z-spectra at 3.5 ppm from the water peak (Zhou et al., 2003a). Intracellular pH (pH_i) was obtained by using the formula (Zhou et al., 2003b)

$$pH_i = \log\left(\Delta APTR / 5.73 + 10^{-2.29}\right) + 9.4 . \quad (36)$$

In this calculation pH_i of 7.11 was assumed for a normal brain. In study **IV** the Z-spectra were obtained by saturating 14 offset frequencies around the free water peak for 5 s with a train of 2.0 ms long 180° Gauss pulses with zero interpulse delay (γB_1 = 50 Hz, TR = 10 s, TE = 6 ms).

4.2.8 Spectroscopy

^{1}H MRS were acquired in the study **I** with an adiabatic SE based water suppressed LASER (Localization by Adiabatic Selective Refocusing) technique (Garwood and DelaBarre, 2001) (TR = 4 s, TE = 30 ms). The sweep width was 2.5 kHz with 4000 data points. The voxel size was 3 mm x 3 mm x 4 mm covering the ischemic striatum. A localized fast automatic shimming (FASTMAP) technique (Gruetter, 1993) was used before acquiring spectra.

From the spectroscopic data the relation between lactate and total creatine was measured. Creatine was used as an internal concentration reference by assuming its cerebral concentration of 10.8 mmol/kg (Macri et al., 2006). The concentration for lactate ([*Lac*]) was used to calculate the intracellular pH (pH_i) (Katsura et al., 1992) from

$$pH_i = -0.0335[Lac] + 6.83. \quad (37)$$

4.3 Data analysis

Data were analyzed mainly using in house written Aedes analysis software (www.aedes.uku.fi) and other in house written software in the Matlab environment (The MathWorks, Natick, MA, USA). Spectroscopy data in study **I** were analyzed using jMRUI software (www.mrui.uab.es/mrui).

In study **III** a two site exchange (2SX) model was fitted to the measured relaxation rate $R_{1\rho}$ and $R_{2\rho}$ values ($R_n = 1/T_n$) using Levenberg-Marquardt nonlinear least squares regression algorithm.

In study **IV** a multiparameter linear correlation was used to find correlation between several individual and combinations of MRI parameters with viable cells.

Statistical differences between ipsi- and contralateral sides were calculated using a paired t-test (**I**, **III**, **IV**) and between ischemic and control animals with a one sample t-test (**I**) with Bonferroni adjustment for multiple comparisons. Values are expressed as mean ± standard error of mean (SEM) (**I**, **II**) or mean ± standard deviation (SD) (**III**, **IV**).

5 RESULTS

5.1 Amide proton transfer ratio and pH in ischemia

The relationship between the APTR and intracellular pH, as calculated from tissue lactate concentration, was examined in the rat MCAo model of focal cerebral ischemia. APTR was computed from the asymmetry in the Z-spectrum, and lactate by ^{1}H NMR spectroscopy. Diffusion and $T_{1\rho}$ MRI were also acquired to determine the severity of ischemia.

Twelve animals with focal cerebral ischemia were studied; 10 of the rats showed severe ischemia as revealed by a decrease in D_{av} by more than 25% at 60 min of MCAo (**I**: Fig. 2a). In seven animals the D_{av} value remained low after removal of the occluder, but three rats showed a small recovery of diffusion towards the values of the contralateral non-ischemic side. The diffusion images were consistent with previously reported studies of cerebral ischemia. $T_{1\rho}$ relaxation time increased by 9% at 60 min of MCAo continuing to increase even during the reperfusion, as expected from irreversible ischemia (**I**: Fig. 2b). In two of the three animals showing recovery in D_{av} during reperfusion $T_{1\rho}$ returned towards the non-ischemic value. These two rats showed mild ischemic damage.

APTR showed a significant decrease during the MCAo as compared to the contralateral hemisphere (**I**: Fig. 4a). The abnormal APTR values returned back to normal during reperfusion. pH_i was 6.71 ± 0.19 in agreement with previous data from a similar stroke model of normoglycemic rats (Zhou et al., 2003b). The drop in pH_i was 0.3 ± 0.2 units during ischemia (**I**: Table 2). Following reperfusion the amount of lactate started to decrease (**I**: Fig. 2b).

Lactate concentration in the ischemic side of the brain was measured to be 16 ± 7 mmol/kg whereas no lactate could be detected in the contralateral side. The lactate concentration translated to a pH_i of 6.3 ± 0.2 in ischemic brain, thus a drop by 0.8 ± 0.2 units (using Eq (37)). The lactate concentration remained high during ischemia and started to slowly decrease showing significant change ($p < 0.05$) only after 2 hours of reperfusion.

The data showed a significant difference between the estimated decrease in pH_i as determined from lactate and APTR. However, there was a significant correlation between APTR and pH_i during the early minutes of ischemia, but in the later time points APTR seemed to underestimate the pH_i change. Cellular acidification therefore seems to be a significant factor affecting APTR during ischemia, but other physicochemical factors simultaneously contribute to the APTR during acute stroke.

5.2 Hemorrhage and ischemia development in the Rose Bengal model of stroke

Temporal profiles of hemorrhage and edema in cerebral stroke were evaluated and the sensorimotor impairment assessed in the photochemical rat stroke model. Lesion volume, edema and bleeding were measured by T_2 and T_2* MRI daily for 10 days and correlated with functional outcome during the follow-up.

In ischemic rats a consistent ipsilateral lesion was detected by day 1 post MCAo (**II**: Fig. 1A). An increase in absolute T_2 was evident by 1 day post-insult (**I**: Fig. 2B), but no signs of hemorrhage were evident in the T_2* images. Bleeding produced signal decrease in T_2* MRI between 3 and 8 days post-insult suggesting vascular breakdown. The presence of bleeding was confirmed by histological staining at day 10. Sensorimotor impairment was evaluated in ischemic rats at days 1, 5 and 10 (**II**: Fig. 2C). Their functional recovery was gradual, coinciding with the resolution of edema and emergence of hemorrhage. It turned out to be difficult to quantitatively assess how MRI observations and sensorimotor defects were interrelated.

Evolving hemorrhage is clearly present in the Rose Bengal model of cerebral ischemia. Late appearance of hemorrhage suggests that it may be linked to the maturation of the lesion rather than to acute leakage in the blood-brain barrier.

5.3 Changes in water pools during ischemia

Rotating frame MRI contrasts, recalled either by means of CW or adiabatic HS pulses, were used to assess their ability to detect hyperacute ischemia in the brain. Irreversible and severe ischemia (D_{av} decreased by 20%) was evident after the 90 minute MCAo (**III**: Fig. 2). By 60 minutes of the MCAo, in contrast to T_2, the $T_{1\rho}$ and $T_{2\rho}$ relaxation time values were significantly increased and continued to increase throughout the follow-up despite the retraction of the occluder (**III**: Fig. 3A, 3B). A clear difference was seen between the $T_{1\rho}$ and $T_{2\rho}$ relaxation times and between HS*n*- and CW-type relaxation times. CW-$T_{1\rho}$ and the HS*n*-$T_{1\rho}$ with high *n* were the most sensitive to ischemic changes with ~10% increase in the relaxation times by 60 minutes and ~15% by 150 minutes of MCAo (**III**: Table 2). An advantage of using HS*n* pulses compared to the CW-technique in $T_{1\rho}$-MRI is the decreased SAR, which was measured to be 81%, 37% and 21% lower using HS1, HS4, and HS8 pulses respectively.

The threshold based analysis, assessing the progression in the MRI contrast values in pixels, showed an increase in the number of pixels with increased relaxation time values (apart from T_2 by 60 minutes) and decrease in diffusion coefficient values as compared with the contralateral non-ischemic brain (**III**: Fig. 5). This demonstrated the spatiotemporal progression of the lesion despite retraction of the occluder thread.

The two site exchange (2SX) model was used to obtain information from changes in water dynamics, i.e. the water pools and the correlation times during permanent MCAo. Significant differences in the fitted model parameters were evident in the lesion area compared to the contralateral normal tissue. The relative size of the free water pool increased in the ischemic brain, while the rotational correlation time of the bound water pool decreased. The exchange correlation time increased in the ischemic tissue as well.

5.4 Correlating stroke lesion outcome with MRI data

Multi-parametric MRI data after 60 minutes of MCAo were correlated with histological outcome determined at 24 hours post occlusion. Severely ischemic animals were divided into two groups based on the size of the lesion as follows: (a) striatal (core) lesion and (b) lesion area that expanded to somatosensory cortex. The expansion area was considered as penumbral area, in which the lesion developed during the 24 hours of the ischemic insult.

A drop in D_{av} and CBF by 30 - 40% and 60 - 70% respectively was seen at 30 min post MCAo followed by a moderate recovery towards normal (contralateral) values upon reperfusion in all ischemic areas (**IV**: Fig. 3). However, during reperfusion the cortical areas that later developed infarction often showed recovery of CBF with an overshoot followed by a secondary decline in CBF. In cortical areas that showed only a small response to reperfusion, CBF gradually returned to normal physiological values and histological lesion was not detected at 24 hours.

CW and HS8 type $T_{1\rho}$ were chosen for this study based on their high inherent sensitivity to ischemia (**III**). Both CW and HS8 $T_{1\rho}$ MRI showed the ischemia in the core tissue as early as 30 minutes post MCAo, when an approximate 4 - 5% increase in the relaxation times was detected (**IV**: Fig. 3). These increases agree with those determined previously in irreversible ischemia (Gröhn et al., 2003) with a B_1 field of 0.4 G. After 60 - 90 minutes post-ischemia, T_2 and $T_{1\rho}$ relaxation times showed similar increase. T_1 showed an increase at 30 minutes post-MCAo in the ischemic tissue. In cortical areas T_1 was able to differentiate the irreversibly ischemic area from 30 min post MCAo onward. CBF showed a fast recovery upon reperfusion, but it was not able to distinguish between damaged and recoverable brain tissue.

The APTR values, collected during reperfusion, slowly recovered. Assuming negligible changes both in content of amide protons and tissue water under these experimental conditions, pH can be considered as the key factor affecting proton exchange rate. Thus, the change in APTR values translated (Zhou et al., 2003b) to a decrease in pH_i of 0.4 pH units. Histology at 24 hours showed that the number of viable cells decreased by 50% in the ischemic lesion core and by 40% in the cortical lesion area, while no significant changes were evident in the lesion free cortex on the ipsilateral and contralateral side.

Considering the striatum as the ischemic core, the single MRI parameter, as determined 30 minutes post MCAo with best correlation with cellular outcome, was CBF. Using a multi-parameter correlation approach, by creating a linear combination with diffusion or any of the relaxation parameters, only a slight increase in the correlation coefficient was obtained (**IV**: Tables 1, 2 and 3). At the later time points, CW-$T_{1\rho}$ showed the best correlation with histological outcome. Again, combining CBF with any of the relaxation parameters slightly increased the correlation coefficient. In the cortical areas correlation with histological outcome was low even with the multi-parameter approach. Using several MRI parameters improved prediction of outcome post-ischemia, but this improvement appears to vary from one anatomical region to the other. High accuracy in predicting the fate of the ischemic core can be achieved using two or three MRI parameters. With penumbral tissue any single MRI contrast has only a low correlation, but with a multi-parameter approach this correlation may be improved to ~0.8.

6 DISCUSSION

Deep understanding of the biochemical, biophysical and cellular events that take place in the brain in response to ischemia is likely to advance implementation of intervention procedures directed to protect the brain from damage and/or expedite the recovery of the brain. Physicochemical events, including time-dependent changes in the water pools and exchange times give a glimpse into this realm. Novel MRI techniques provide us with new ways to probe these and several other biophysical factors contributing to ischemic damage. It is anticipated that MRI, by providing access to stroke evolution, may help to guide the use of investigational treatment strategies to prevent and alleviate the effects of ischemic damage to brain functions.

In the current study several conventional and novel MRI contrasts were used to assess the dynamic processes that take place in brain parenchyma during and after ischemia. In the MCAo model used, the striatum was considered to constitute the ischemic core. Apart from the early lesion expansion in the striatal area, brain cortex was perceived as the ischemic penumbra, as the lesion encompassed the insular and piriform cortices and also the somatosensory area at later time points.

6.1 From individual MRI parameters…

^{1}H MRI signal arises from water *in vivo*, which undergoes multiple types of interactions with proteins, macromolecules and various cell structures. Inherent mobility of water and interactions with biomolecules and cellular structures strongly influence biophysical properties of biological water and thus, MRI signal. Therefore convoluted methods have to be applied to segregate information from MRI signal. Separating “magnetically” different environments of water protons in tissue may provide means to infer a wide variety of information. Selecting from a wealth of MRI contrasts through available pulse sequences probing inherently differing dynamic components, a vast variety of biological information can be obtained by observing the water signal.

Conventional MRI contrasts, such as T_2, diffusion and perfusion, have been available to assess brain status and/or evolution of damage due to ischemia (van Bruggen et al., 1994). Together these contrasts give unprecedented information from the physiological state of tissue. However, predictive value by diffusion and perfusion MRI for long term outcome is not optimal (Sobesky et al., 2005). This is due to several reasons, such as possibly reversible tissue changes in diffusion MRI after cytotoxic edema resolves (Minematsu et al., 1992). Perfusion on the other hand rapidly reacts to blood flow changes and thus gives predictive value only in situations where perfusion defect is long-lasting for an extended period of time. Naturally, in clinical situations these

parameters give essential information about the present state - a snapshot - of the ischemic progression. But the MRI penumbra, as defined by the mismatch between diffusion and perfusion, can have both irreversibly damaged tissue and area of benign oligemia (Sorensen et al., 1996). Imaging methods are researched capable to reveal heterogeneous area and to reveal treatable tissue, and perhaps beyond that, to indicate directly the energy state of cells. At present it is not feasible to predict the outcome of an individual neural cell by MRI due to low inherent spatial resolution. On the other hand, it may also be impractical clinically and pre-clinically, since the results of such predictions are statistical and even with available MRI resolution, the predictions give plenty of information, for example when treatment responses are evaluated.

Here diffusion was the key MRI contrast (a) to delineate acute ischemia anatomically and (b) indicate severity of ischemia. Ischemic lesion, as indicated by diffusion MRI, developed in animals with individual temporal characteristics, exhibiting biological variation. The smallest lesions only partially covered the striatum whereas the largest extended through amygdala up to the somatosensory cortex. The variability in collateral vasculature and other physiological factors, such as sensitivity to ischemia, may contribute to the size of the ischemic lesion. As far as the CBF is concerned, the biological variation in the diameter of the occluded vessel relative to the occluding thread may lead to some seeping. A further factor that may influence ischemia volume in acute phase is body temperature. The core temperature was kept within physiological range under halothane or isoflurane anesthesia throughout each experiment to keep their possible neuroprotective effects minimal.

T_2 MRI provides information about the mismatch of oxygen delivery and consumption within the first minutes of lowered CBF through a negative BOLD effect (Calamante et al., 1999a; Gröhn et al., 1998). However, by 30 minutes of MCAo there was no difference in T_2 between non-ischemic and ischemic tissue despite on-going ischemia and thus alternative MRI methods are needed to reveal compromised tissue status. Only after 90 minutes of ischemia increased T_2 values were detected marking severe ischemia in tissue that will be irreversibly damaged. In clinical settings 1.5-2 hours is a possible time window from the onset of ischemia for a stroke patient to be exposed to MRI scans and T_2 can potentially give information about the developing vasogenic edema (Kato et al., 1986; van der Toorn et al., 1994).

T_2* MRI is a potent imaging technique to visualize hemorrhage inside and surrounding the ischemic area. It adds a key diagnostic tool for clinical practice providing a contraindication to thrombolytic therapies (Eckman et al., 2003). However, bleeding is not just a complication of ischemic damage, but the perilesional hemorrhage can be an integral mechanism of recovery process for the lesion that may expedite healing of the brain tissue.

T_1 relaxation time increases within seconds after an ischemic insult (Calamante et al., 1999b; Kettunen et al., 2000), contrary to the studies published in 80s (Buonanno et al., 1983; Kato et al., 1985). The current study agrees with the observations by Calamante and Kettunen that T_1 is an early MRI indicator of ischemia. The T_1 value remained high after the initial increase, with no apparent change within the next few hours. Because of this temporal pattern, T_1 MRI fails to provide information about the age of the lesion in the acute phase of ischemia. Increased T_1 is likely to be partially due to the increased overall water content in ischemic brain, but as vasogenic edema starts only a few hours after ischemic insult, it may not be the predominant factor (Calamante et al., 1999a). The fact that proton density does not change during the early ischemia supports this conclusion. Several biophysical factors affecting T_1 such as temperature, and blood flow (Calamante et al., 1999a; Ewing et al., 1999; Lin et al., 2000), but no clear consensus prevails about their quantitative contributions to the early ischemic T_1 increase (Barber et al., 2005).

The rotating frame MRI contrasts exhibit sensitivity to slow molecular motions and they provide a way to exploit the exchange interaction between free and bound water for MRI. The current study demonstrates great potentials for rotating frame relaxation times to detect acute stroke. $T_{1\rho}$ relaxation time showed an early increase to ischemia and a good correlation with long-term tissue outcome (Gröhn et al., 1999). $T_{1\rho}$ showed linear increase in the acute phase and by doing so is a potential MRI marker for the age of the lesion. Furthermore, $T_{1\rho}$ has a potential to predict the final lesion size. $T_{2\rho}$ of brain tissue is influenced by water diffusion and exchange processes between different chemical environments (Michaeli et al., 2004). Against these facts, despite the observed inability of $T_{2\rho}$ MRI to reveal ischemic damage during the evolution of infarction, it can add information about tissue status together with $T_{1\rho}$. It should be stressed that sensitivity of $T_{2\rho}$ to ischemia can be modified by changing the SL preparation pulses and thereby, introducing more possibilities to modulate the contrast *in vivo*.

The main caveat with the use of rotating frame MRI techniques in the clinical setting concerns the SAR limits. More work is needed to optimize these techniques to achieve high enough contrast within workable B_1 field strengths. Instead of using the CW approach, adiabatic pulses, such as the HS*n* type pulses, can be used to lower the SAR. Another concern is the homogeneity of the SL field, which is hard to accomplish for a head-sized target. Despite these issues, rotating frame techniques are steadily gaining attention in pre-clinical MRI, but still more research is needed for them to gain a steady place in clinical settings (Gröhn et al., 2005; Michaeli et al., 2009; Sierra et al., 2008).

Another investigational contrast, APTR, with its sensitivity to pH can give valuable information about the intracellular state and thus it adds a valuable part to the collection of MRI tools for ischemic tissue analysis (Sun et al., 2007b). Temporary ischemia causes an increase in MT that is partly caused by increased water content and changes in the water-macromolecule interface, due to

proteolysis, etc. As pH is a major factor in modulation of chemical exchange rate, as it varies with the concentration of H^+ and OH^- ions in tissue, a decrease in pH leads to a decrease in the exchange between water and the macromolecule exchangeable chemical groups. A decrease in pH has also been reported for apoptotic cells, thus APTR is a potential apoptosis marker. However, there are other factors affecting pH, such as temperature and the sensitivity to B_1 and B_0 inhomogeneities that would complicate the analysis (Sun et al., 2007a).

6.2 …through understanding the mechanism underpinning changes…

In ischemic tissue there is a decrease of free water and increase of macromolecule bound water due to cell swelling (Barbier et al., 2005). Ischemia leads to a decrease in the extracellular volume, which may contribute to an decrease in ADC (Moseley et al., 1990; van der Toorn et al., 1996). Rotating frame contrasts have shown sensitivity to changes that occur during both apoptotic and necrotic cell death (Sierra et al., 2008). Further studies are needed to evaluate if this sensitivity can be exploited in the analysis of ischemic tissue. After a short transient MCAo selective and incomplete cell death is observed in experimental models (De Girolami 1984). This may be due to variations in the vulnerability of different neurons, astrocytes, glial and endothelial cells. Most neurons are usually damaged, due to their high vulnerability to ischemia. A difference in the regional sensitivity to stroke and oxygen and glucose deprivation is feasible due to factors like collateral circulation and different cellular energy capacity (mitochondrial capacity).

The MCAo model is a commonly used method to study cerebral ischemia in rodents. It produces reasonably reproducible lesions yet with some variation due to physiological differences between individual animals. The latter feature of the MCAo model resembles what is evident with clinical cases. The Rose Bengal model, on the other hand, is well suited for producing a local stroke lesion when excellent reproducibility is required. However, this model creates severe damage with still unknown complications (cf. hemorrhage) and is not easy to interpret clinically. Still, the Rose Bengal model provides a model to study the hemorrhage associated with vasogenic edema. Preclinical stroke models may not fully capture all the clinical aspects. Nevertheless, animal models are valuable for researching new stroke imaging techniques.

Several of the studied MRI parameters show time-dependent changes to ischemia. Early diffusion changes and late T_2 changes are easy to measure as they exceed 20% in size. Similarly $T_{1\rho}$ after an hour of ischemia starts to approach a similar magnitude of change. Acquiring data for several MRI parameters in a short time with acceptable contrast-to-noise ratio is challenging. This is especially problematic with the APTR and ASL data. The ASL measurement is based on a small difference in two sets of images taking much longer time to collect than the T_2 or $T_{1\rho}$ measurements.

Consequently, to obtain a 30 minute time resolution in this type of experiments is difficult. In our study (**IV**) APTR MRI had to be left out due to this fact, and APTR data was collected only during the scans with 60 minute cycling time. This low temporal resolution was chosen to assure high signal-to-noise ratio in images leading to good contrast-to-noise ratio for multi-parametric analyses.

6.3 …to multiparametric MR imaging

The present data show that multiparametric MRI could improve regional and statistical prediction of tissue outcome, which is consistent with previously published work (Ding et al., 2004; Lu et al., 2005; Wu et al., 2007). ROI analysis showed improvement of prediction using two or three MRI parameters compared to what was obtained with a single MRI parameter. Pixel-by-pixel correlations between each MR image were analyzed in order to better characterize the changes, but due to large statistical variation between animals exposed to 60 minutes of MCAo the results did not provide improvement relative to the ROI based approach. A possible reason for this result could lie in changed morphology due to tissue swelling that distorts brain structures and makes pixel-by-pixel matches from time point to another as well as matches to histology somewhat uncertain.

Our data suggest that information provided by multiparametric MRI to predict tissue outcome may help to evaluate efficacy of new treatment strategies non-invasively in experimental models. It is evident that the combination of novel MRI contrasts, particularly $T_{1\rho}$ with established ones together with advanced image processing may provide needed tools to translate these techniques into clinical settings to aid in decision making for the optimal treatment protocols of stroke patients. Imaging data including the site of occlusion, age of ischemia, presence of possible hemorrhage and presence of salvageable tissue are perhaps the key aspects that benefit the critical care of stroke patients.

In 2008 a recommendation was issued by an international working party to standardize stroke imaging (Wintermark et al., 2008). The recommendation for baseline MRI included a set of DWI, MRA, T_2*-WI, PWI, T_2-WI and an optional T_1-WI. The rationale behind these MRI techniques was to address four main points: the initial perfusion and tissue state, effect of intervention, presence of hemorrhage and assessment of outcome. If adapted into full clinical use, this MRI protocol will produce quickly a vast database with good statistical value for both clinicians and stroke researchers around the world.

6.4 Future directions

Imaging of stroke by MR-based techniques has come a long way from the groundbreaking studies published in the 80s. Those studies showed that T_1 and/or T_2-MRI can delineate the stroke lesion *in vivo* hours after the insult (Kato et al., 1986; Naruse et al., 1986). The next milestone was the introduction of DWI to brain imaging, providing a means to detect brain ischemia within minutes after the onset (Moseley et al., 1990). These achievements were followed by inclusion of perfusion MRI into assessment of hemodynamics in stroke by Sorensen and coworkers (Sorensen et al., 1996), with a goal to reveal the tissue at risk of infarction. The recent years have witnessed a march of further developments of MRI techniques for stroke imaging, including $T_{1\rho}$ (Gröhn et al., 1999) and APTR (Zhou et al., 2003b). It is justified to claim that today MRI provides an unprecedented imaging platform for both preclinical and clinical stroke communities. The MRI techniques above, as complemented with those investigated in the present study, are expected to promote development of optimized treatment protocols for stroke, such as clinical hypothermia, pharmacological agents and other neuroprotective strategies (Durukan and Tatlisumak, 2007; Pignataro et al., 2009). These provide momentum for the development of new and sensitive imaging techniques to reveal salvageable brain tissue in acute stroke. All the MRI contrasts used in the present study provide complementary information about the water dynamics in cerebral tissue during acute ischemic stroke that may potentially be used to determine reversibility of tissue status.

More specific and sensitive MRI techniques for parameters, such as pH, are under development (Närväinen et al., 2009; Sun et al., 2007b) and they are expected to improve delineation of ischemic damage and tissue viability. Techniques, such as fMRI, pharmacological MRI (phMRI), diffusion tensor imaging (DTI) and molecular imaging using targeted contrast agents may provide additional information for experimental stroke studies and later in clinical environment (Barber et al., 2004; Heckl, 2007; Hoehn et al., 2001; Sotak, 2002). Many of the MRI contrasts above are sensitive to the tissue changes of cerebral ischemia. Similarly, other areas of biomedical research, such as bone and cartilage imaging ($T_{1\rho}$), cancer research ($T_{1\rho}$ and APTR) and other neurodegenerative diseases ($T_{1\rho}$ and $T_{2\rho}$) are likely to benefit from these contrast developments. A challenge remains to image dynamic processes, such as hypoxia at the macroscopic level and apoptosis or gene expression at the microscopic level.

7 SUMMARY AND CONCLUSIONS

In this project we have assessed the complementary value of several established and investigational MRI contrasts during and after acute cerebral ischemia of the rat. The latter included sensitivities of rotating frame relaxations that were assessed for acute stroke detection.

The complementary nature of MRI contrasts was evident in all of these studies, as they all gain contributions from complex dynamic factors taking place in the brain parenchyma during the evolution of ischemic stroke.

The key findings of these studies were:

1. Amide proton transfer ratio (APTR) is a novel and invaluable MRI contrast to explore pathologic changes during ischemia. Decrease in APTR during MCA occlusion and slow recovery during reperfusion suggest that the sensitivity of APTR is not only due to the tissue acidification but also to other physicochemical factors.

2. Hemorrhage following cortical infarct coincided with the improvement of the sensorimotor functions. This suggests that the subacute bleeding around the cortical infarct area does not prevent functional recovery.

3. Sensitivity of the rotating frame MRI contrasts can be modified using different preparation pulse sequences. CW-$T_{1\rho}$ and HSn-$T_{1\rho}$ (with large n) were the most sensitive techniques to detect hyperacute stroke. The relaxation changes appear to be due to increased tissue water content, increase in the macromolecule-bound water pool and a change in water exchange behavior.

4. Monitoring the progression of ischemic lesion is feasible using multiparametric MRI. Combining the data from 3-4 MRI parameters that describe the hemodynamic and parenchymal changes in tissue during ischemia makes the prediction of lesion outcome possible, with high accuracy.

5. The novel MRI contrasts, APTR and the rotating frame relaxation times are likely to benefit pre-clinical stroke research. Due to the present SAR limits further studies are needed to assess their clinical applicability.

8 REFERENCES

Abragam, A. (1961). The Principles of Nuclear Magnetism. (Oxford: The Clarendon Press).

Allen, K., Busza, A. L., Crockard, H. A., Frackowiak, R. S. J., Gadian, D. G., Proctor, E., Ross Russell, R. W., and Williams, S. R. (1988). Acute cerebral ischaemia: concurrent changes in cerebral blood flow, energy metabolites, pH, and lactate measured with hydrogen clearance and ^{31}P and ^{1}H nuclear magnetic resonance spectroscopy. III. Changes following ischaemia. J Cereb Blood Flow Metab *8*, 816-821.

Allerhand, A., and Gutowsky, H. S. (1964). Spin-echo NMR studies of chemical exchange. I. Some general aspects. J Chem Phys *41*, 2115-2126.

Alsop, D. C., and Detre, J. A. (1996). Reduced transit-time sensitivity in noninvasive magnetic resonance imaging of human cerebral blood flow. J Cereb Blood Flow Metab *16*, 1236-1249.

Amantea, D., Nappi, G., Bernardi, G., Bagetta, G., and Corasaniti, M. T. (2009). Post-ischemic brain damage: pathophysiology and role of inflammatory mediators. Febs J *276*, 13-26.

Anzalone, N. (2005). Contrast-enhanced MRA of intracranial vessels. Eur Radiol *15 Suppl 5*, E3-10.

Aronowski, J., Strong, R., and Grotta, J. C. (1997). Reperfusion injury: demonstration of brain damage produced by reperfusion after transient focal ischemia in rats. J Cereb Blood Flow Metab *17*, 1048-1056.

Astrup, J., Siesjö, B. K., and Symon, L. (1981). Thresholds in cerebral ischemia: the ischemic penumbra. Stroke *12*, 723-725.

Astrup, J., Symon, L., Branston, N. M., and Lassen, N. A. (1977). Cortical evoked potential and extracellular K+ and H+ at critical levels of brain ischemia. Stroke *8*, 51-57.

Balaban, R. S., and Ceckler, T. L. (1992). Magnetization transfer contrast in magnetic resonance imaging. Magn Reson Q *8*, 116-137.

Barber, P. A., Davis, S. M., Darby, D. G., Desmond, P. M., Gerraty, R. P., Yang, Q., Jolley, D., Donnan, G. A., and Tress, B. M. (1999). Absent middle cerebral artery flow predicts the presence and evolution of the ischemic penumbra. Neurology *52*, 1125-1132.

Barber, P. A., Foniok, T., Kirk, D., Buchan, A. M., Laurent, S., Boutry, S., Muller, R. N., Hoyte, L., Tomanek, B., and Tuor, U. I. (2004). MR molecular imaging of early endothelial activation in focal ischemia. Ann Neurol *56*, 116-120.

Barber, P. A., Hoyte, L., Kirk, D., Foniok, T., Buchan, A., and Tuor, U. (2005). Early T1- and T2-weighted MRI signatures of transient and permanent middle cerebral artery occlusion in a murine stroke model studied at 9.4T. Neurosci Lett *388*, 54-59.

Barbier, E. L., Liu, L., Grillon, E., Payen, J. F., Lebas, J. F., Segebarth, C., and Remy, C. (2005). Focal brain ischemia in rat: acute changes in brain tissue T1 reflect acute increase in brain tissue water content. NMR Biomed *18*, 499-506.

Barrett, T., Brechbiel, M., Bernardo, M., and Choyke, P. L. (2007). MRI of tumor angiogenesis. J Magn Reson Imaging *26*, 235-249.

Basser, P. J., Mattiello, J., and Le Bihan, D. (1994a). Estimation of the effective self-diffusion tensor from the NMR spin echo. J Magn Reson B *103*, 247-254.

Basser, P. J., Mattiello, J., and Le Bihan, D. (1994b). MR diffusion tensor spectroscopy and imaging. Biophys J *66*, 259-267.

Basser, P. J., and Pierpaoli, C. (1996). Microstructural and physiological features of tissues elucidated by quantitative-diffusion-tensor MRI. J Magn Reson B *111*, 209-219.

Behar, K. L., Rothman, D. L., and Hossmann, K. A. (1989). NMR spectroscopic investigation of the recovery of energy and acid-base homeostasis in the cat brain after prolonged ischemia. J Cereb Blood Flow Metab *9*, 655-665.

Beilharz, E. J., Williams, C. E., Dragunow, M., Sirimanne, E. S., and Gluckman, P. D. (1995). Mechanisms of delayed cell death following hypoxic-ischemic injury in the immature rat: evidence for apoptosis during selective neuronal loss. Mol Brain Res *29*, 1-14.

Belliveau, J. W., Kennedy, D. N., McKinstry, R. C., Buchbinder, B. R., Weisskoff, R. M., Cohen, M. S., Vevea, J. M., Brady, T. J., and Rosen, B. R. (1991). Functional mapping of human visual cortex by magnetic resonance imaging. Science *254*, 716-719.

Belliveau, J. W., Rosen, B. R., Kantor, H. L., Rzedzian, R. R., Kennedy, D. N., McKinstry, R. C., Vevea, J. M., Cohen, M. S., Pykett, I. L., and Brady, T. J. (1990). Functional cerebral imaging by susceptibility-contrast NMR. Magn Reson Med *14*, 538-546.

Benveniste, H., Hedlund, L. W., and Johnson, G. A. (1992). Mechanism of detection of acute cerebral ischemia in rats by diffusion-weighted magnetic resonance microscopy. Stroke *23*, 746-754.

Berkelbach van der Sprenkel, J. W., Luyten, P. R., van Rijen, P. C., Tulleken, C. A. F., and den Hollander, J. A. (1988). Cerebral lactate detected by regional proton magnetic resonance spectroscopy in a patient with cerebral infarction. Stroke *19*, 1556-1560.

Bloch, F., Hansen, W. W., and Packard, M. E. (1946). Nuclear induction. Phys Rev *69*, 127.

Borcard, B. (1984). Field dependence of relaxation times. Nuclear magnetic relaxation dispersion. Prog Nucl Med *8*, 47-54.

Borlongan, C. V., Tajima, Y., Trojanowski, J. Q., Lee, V. M., and Sanberg, P. R. (1998). Transplantation of cryopreserved human embryonal carcinoma-derived neurons (NT2N cells) promotes functional recovery in ischemic rats. Exp Neurol *149*, 310-321.

Borthakur, A., Sochor, M., Davatzikos, C., Trojanowski, J. Q., and Clark, C. M. (2008). T1rho MRI of Alzheimer's disease. Neuroimage *41*, 1199-1205.

Borthakur, A., Wheaton, A. J., Gougoutas, A. J., Akella, S. V., Regatte, R. R., Charagundla, S. R., and Reddy, R. (2004). In vivo measurement of T1rho dispersion in the human brain at 1.5 tesla. J Magn Reson Imaging *19*, 403-409.

Bottomley, P. A., Foster, T. H., Argersinger, R. E., and Pfeifer, L. M. (1984). A review of normal tissue hydrogen NMR relaxation times and relaxation mechanisms from 1-100 MHz: dependence on tissue type, NMR frequency, temperature, species, excision, and age. Med Phys *11*, 425-448.

Branston, N. M., Strong, A. J., and Symon, L. (1977). Extracellular potassium activity, evoked potential and tissue blood flow. Relationships during progressive ischaemia in baboon cerebral cortex. J Neurol Sci *32*, 305-321.

Broughton, B. R., Reutens, D. C., and Sobey, C. G. (2009). Apoptotic mechanisms after cerebral ischemia. Stroke *40*, e331-339.

Bryant, R. G. (1996). The dynamics of water-protein interactions. Annu Rev Biophys Biomol Struct *25*, 29-53.

Buonanno, F. S., Pykett, I. L., Brady, T. J., Vielma, J., Burt, C. T., Goldman, M. R., Hinshaw, W. S., Pohost, G. M., and Kistler, J. P. (1983). Proton NMR imaging in experimental ischemic infarction. Stroke *14*, 178-184.

Busto, R., Dietrich, W. D., Globus, M. Y., Valdes, I., Scheinberg, P., and Ginsberg, M. D. (1987). Small differences in intraischemic brain temperature critically determine the extent of ischemic neuronal injury. J Cereb Blood Flow Metab *7*, 729-738.

Busza, A. L., Allen, K. L., King, M. D., van Bruggen, N., Williams, S. R., and Gadian, D. G. (1992). Diffusion-weighted imaging studies of cerebral ischemia in gerbils. Potential relevance to energy failure. Stroke *23*, 1602-1612.

Calamante, F., Lythgoe, M. F., Pell, G. S., Thomas, D. L., King, M. D., Busza, A. L., Sotak, C. H., Williams, S. R., Ordidge, R. J., and Gadian, D. G. (1999a). Early changes in water diffusion, perfusion, T_1, and T_2 during focal cerebral ischemia in the rat studied at 8.5 T. Magn Reson Med *41*, 479-485.

Calamante, F., Thomas, D. L., Pell, G. S., Wiersma, J., and Turner, R. (1999b). Measuring cerebral blood flow using magnetic resonance imaging techniques. J Cereb Blood Flow Metab *19*, 701-735.

Carano, R. A., Li, F., Irie, K., Helmer, K. G., Silva, M. D., Fisher, M., and Sotak, C. H. (2000). Multispectral analysis of the temporal evolution of cerebral ischemia in the rat brain. J Magn Reson Imaging *12*, 842-858.

Carano, R. A., Takano, K., Helmer, K. G., Tatlisumak, T., Irie, K., Petruccelli, J. D., Fisher, M., and Sotak, C. H. (1998). Determination of focal ischemic lesion volume in the rat brain using multispectral analysis. J Magn Reson Imaging *8*, 1266-1278.

Carden, D. L., and Granger, D. N. (2000). Pathophysiology of ischaemia-reperfusion injury. J Pathol *190*, 255-266.

Carr, H. Y., and Purcell, E. M. (1954). Effects of diffusion on free precession in nuclear magnetic resonance experiments. Physical Rev *94*, 630-638.

Cho, S., and Kim, E. (2009). CD36: a multi-modal target for acute stroke therapy. J Neurochem *109 Suppl 1*, 126-132.

Clark, C. A., and Le Bihan, D. (2000). Water diffusion compartmentation and anisotropy at high b values in the human brain. Magn Reson Med *44*, 852-859.

Cohen, P. J., Alexander, S. C., Smith, T. C., Reivich, M., and Wollman, H. (1967). Effects of hypoxia and normocarbia on cerebral blood flow and metabolism in conscious man. J Appl Physiol *23*, 183-189.

Combs, D. J., Dempsey, R. J., Maley, M., Donaldson, D., and Smith, C. (1990). Relationship between plasma glucose, brain lactate, and intracellular pH during cerebral ischemia in gerbils. Stroke *21*, 936 - 942.

Constable, R. T., Anderson, A. W., Zhong, J., and Gore, J. C. (1992). Factors influencing contrast in fast spin-echo MR imaging. Magn Reson Imaging *10*, 497-511.

Crockard, H. A., Gadian, D. G., Frackowiak, R. S. J., Proctor, E., Allen, K., Williams, S. R., and Russell, R. W. R. (1987). Acute cerebral ischaemia: concurrent changes in cerebral blood flow, energy metabolites, pH, and lactate measured with hydrogen clearance and ^{31}P and ^{1}H nuclear magnetic resonance spectroscopy. II. Changes during ischaemia. J Cereb Blood Flow Metab *7*, 394-402.

Davis, D., Ulatowski, J., Eleff, S., Izuta, M., Mori, S., Shungu, D., and van Zijl, P. C. M. (1994). Rapid monitoring of changes in water diffusion coefficients during reversible ischemia in cat and rat brain. Magn Reson Med *31*, 454-460.

De Crespigny, A. J., Wendland, M. F., Derugin, N., Kozniewska, E., and Moseley, M. E. (1992). Real time observation of transient focal ischemia and hyperemia in cat brain. Magn Reson Med *27*, 391-397.
del Zoppo, G. J. (1998). Clinical trials in acute stroke: why have they not been successful? Neurology *51*, S59-61.
del Zoppo, G. J., Poeck, K., Pessin, M. S., Wolpert, S. M., Furlan, A. J., Ferbert, A., Alberts, M. J., Zivin, J. A., Wechsler, L., Busse, O., and et al. (1992). Recombinant tissue plasminogen activator in acute thrombotic and embolic stroke. Ann Neurol *32*, 78-86.
Denes, A., Ferenczi, S., Halasz, J., Kornyei, Z., and Kovacs, K. J. (2008). Role of CX3CR1 (fractalkine receptor) in brain damage and inflammation induced by focal cerebral ischemia in mouse. J Cereb Blood Flow Metab *28*, 1707-1721.
Derdeyn, C. P., Videen, T. O., Yundt, K. D., Fritsch, S. M., Carpenter, D. A., Grubb, R. L., and Powers, W. J. (2002). Variability of cerebral blood volume and oxygen extraction: stages of cerebral haemodynamic impairment revisited. Brain *125*, 595-607.
Dereski, M. O., Chopp, M., Knight, R. A., Rodolosi, L. C., and Garcia, J. H. (1993). The heterogeneous temporal evolution of focal ischemic neuronal damage in the rat. Acta Neuropathol *85*, 327-333.
Detre, J. A., Leigh, J. S., Williams, D. S., and Koretsky, A. P. (1992). Perfusion imaging. Magn Reson Med *23*, 37-45.
Diegel, J. G., and Pintar, M. M. (1975). Origin of the nonexponentiality of the water proton spin relaxations in tissue. Biophys J *15*, 855-860.
Dienel, G. A., and Hertz, L. (2005). Astrocytic contributions to bioenergetics of cerebral ischemia. Glia *50*, 362-388.
Dietz, R. M., Weiss, J. H., and Shuttleworth, C. W. (2009). Contributions of Ca2+ and Zn2+ to spreading depression-like events and neuronal injury. J Neurochem *109 Suppl 1*, 145-152.
Diller, K. R., and Zhu, L. (2009). Hypothermia Therapy for Brain Injury. Annu Rev Biomed Eng.
Ding, G., Jiang, Q., Zhang, L., Zhang, Z., Knight, R. A., Soltanian-Zadeh, H., Lu, M., Ewing, J. R., Li, Q., Whitton, P. A., and Chopp, M. (2004). Multiparametric ISODATA analysis of embolic stroke and rt-PA intervention in rat. J Neurol Sci *223*, 135-143.
Dirnagl, U., Iadecola, C., and Moskowitz, M. A. (1999). Pathobiology of ischaemic stroke: an integrated view. Trends Neurosci *22*, 391-397.
Dirnagl, U., and Pulsinelli, W. (1990). Autoregulation of cerebral blood flow in experimental focal brain ischemia. J Cereb Blood Flow Metab *10*, 327-336.
Dixon, W. T., Engels, H., Castillo, M., and Sardashti, M. (1990). Incidental magnetization transfer contrast in standard multislice imaging. Magn Reson Imaging *8*, 417-422.
Dringen, R., Gebhardt, R., and Hamprecht, B. (1993). Glycogen in astrocytes: possible function as lactate supply for neighboring cells. Brain Res *623*, 208-214.
Duhamel, G., de Bazelaire, C., and Alsop, D. C. (2003). Evaluation of systematic quantification errors in velocity-selective arterial spin labeling of the brain. Magn Reson Med *50*, 145-153.
Duong, T. Q., Ackerman, J. J. H., Ying, H. S., and Neil, J. J. (1998). Evaluation of extra- and intracellular apparent diffusion in normal and globally ischemic rat brain via ^{19}F NMR. Magn Reson Med *40*, 1-13.
Durukan, A., and Tatlisumak, T. (2007). Acute ischemic stroke: overview of major experimental rodent models, pathophysiology, and therapy of focal cerebral ischemia. Pharmacol Biochem Behav *87*, 179-197.
Easton, J. D., Saver, J. L., Albers, G. W., Alberts, M. J., Chaturvedi, S., Feldmann, E., Hatsukami, T. S., Higashida, R. T., Johnston, S. C., Kidwell, C. S., *et al.* (2009). Definition and evaluation of transient ischemic attack: a scientific statement for healthcare professionals from the American Heart Association/American Stroke Association Stroke Council; Council on Cardiovascular Surgery and Anesthesia; Council on Cardiovascular Radiology and Intervention; Council on Cardiovascular Nursing; and the Interdisciplinary Council on Peripheral Vascular Disease. The American Academy of Neurology affirms the value of this statement as an educational tool for neurologists. Stroke *40*, 2276-2293.
Eckman, M. H., Rosand, J., Knudsen, K. A., Singer, D. E., and Greenberg, S. M. (2003). Can patients be anticoagulated after intracerebral hemorrhage? A decision analysis. Stroke *34*, 1710-1716.
Edelman, R. R., Mattle, H. P., O'Reilly, G. V., Wentz, K. U., Liu, C., and Zhao, B. (1990). Magnetic resonance imaging of flow dynamics in the circle of Willis. Stroke *21*, 56-65.
Englander, S. W., Downer, N. W., and Teitelbaum, H. (1972). Hydrogen exchange. Annu Rev Biochem *41*, 903-924.
Ewing, J. R., Jiang, Q., Boska, M., Zhang, Z. G., Brown, S. L., Li, G. H., Divine, G. W., and Chopp, M. (1999). T_1 and magnetization transfer at 7 Tesla in acute ischemic infarct in the rat. Magn Reson Med *41*, 696-705.
Ferrari, M., Wilson, D. A., Hanley, D. F., and Traystman, R. J. (1992). Effects of graded hypotension on cerebral blood flow, blood volume, and mean transit time in dogs. Am J Physiol *262*, H1908-1914.
Finch, E. D., and Homer, L. D. (1974). Proton nuclear magnetic resonance relaxation measurements in frog muscle. Biophys J *14*, 907-921.
Fogelholm, R., and Baumann, P. (2002). [Treatment of stroke in Finland]. Duodecim *118*, 2523-2525.
Frank, L. R., Wong, E. C., and Buxton, R. B. (1997). Slice profile effects in adiabatic inversion: application to multislice perfusion imaging. Magn Reson Med *38*, 558-564.

Garwood, M., and DelaBarre, L. (2001). The return of the frequency sweep: designing adiabatic pulses for contemporary NMR. J Magn Reson *153*, 155-177.
Grad, J., Mendelson, D., Hyder, F., and Bryant, R. G. (1991). Applications of nuclear magnetic cross-relaxation spectroscopy to tissues. Magn Reson Med *17*, 452-459.
Graham, G. D., Kalvach, P., Blamire, A. M., Brass, L. M., Fayad, P. B., and Prichard, J. W. (1995). Clinical correlates of proton magnetic resonance spectroscopy findings after acute cerebral infarction. Stroke *26*, 225-229.
Granger, D. N., and Korthuis, R. J. (1995). Physiologic mechanisms of postischemic tissue injury. Annu Rev Physiol *57*, 311-332.
Gröhn, H., Michaeli, S., Garwood, M., Kauppinen, R., and Gröhn, O. (2005). Quantitative T(1rho) and adiabatic Carr-Purcell T2 magnetic resonance imaging of human occipital lobe at 4 T. Magn Reson Med *54*, 14-19.
Gröhn, O., Mäkelä, H., Lukkarinen, J., DelaBarre, L., Lin, J., Garwood, M., and Kauppinen, R. (2003). On- and off-resonance T(1rho) MRI in acute cerebral ischemia of the rat. Magn Reson Med *49*, 172-176.
Gröhn, O. H., and Kauppinen, R. A. (2001). Assessment of brain tissue viability in acute ischemic stroke by BOLD MRI. NMR Biomed *14*, 432-440.
Gröhn, O. H., Lukkarinen, J. A., Oja, J. M., van Zijl, P. C., Ulatowski, J. A., Traystman, R. J., and Kauppinen, R. A. (1998). Noninvasive detection of cerebral hypoperfusion and reversible ischemia from reductions in the magnetic resonance imaging relaxation time, T_2. J Cereb Blood Flow Metab *18*, 911-920.
Gröhn, O. H., Lukkarinen, J. A., Silvennoinen, M. J., Pitkänen, A., van Zijl, P. C., and Kauppinen, R. A. (1999). Quantitative magnetic resonance imaging assessment of cerebral ischemia in rat using on-resonance T_1 in the rotating frame. Magn Reson Med *42*, 268-276.
Gröhn, O. H. J., Kettunen, M. I., Mäkelä, H. I., Penttonen, M., Pitkänen, A., Lukkarinen, J. A., and Kauppinen, R. A. (2000a). Early detection of irreversible cerebral ischemia in the rat using dispersion of the MRI relaxation time, $T_{1\rho}$. J Cereb Blood Flow Metab *20*, 1457-1466.
Gröhn, O. H. J., Kettunen, M. I., Penttonen, M., Oja, J. M. E., van Zijl, P. C. M., and Kauppinen, R. A. (2000b). Graded reduction of cerebral blood flow in rat as detected by the nuclear magnetic resonance relaxation time T_2: A theoretical and experimental approach. J Cereb Blood Flow Metab *20*, 316-326.
Grösch, L., and Noack, F. (1976). NMR relaxation investigation of water mobility in aqueous bovine serum albumin solutions. Biochim Biophys Acta *453*, 218-232.
Grubb, R. L., Jr., Derdeyn, C. P., Fritsch, S. M., Carpenter, D. A., Yundt, K. D., Videen, T. O., Spitznagel, E. L., and Powers, W. J. (1998). Importance of hemodynamic factors in the prognosis of symptomatic carotid occlusion. JAMA *280*, 1055-1060.
Grubb, R. L., Jr., Phelps, M. E., Raichle, M. E., and Ter-Pogossian, M. M. (1973). The effects of arterial blood pressure on the regional cerebral blood volume by X-ray fluorescence. Stroke *4*, 390-399.
Gruetter, R. (1993). Automatic, localized in vivo adjustment of all first- and second-order shim coils. Magn Reson Med *29*, 804-811.
Hacke, W., Kaste, M., Bluhmki, E., Brozman, M., Davalos, A., Guidetti, D., Larrue, V., Lees, K. R., Medeghri, Z., Machnig, T., *et al*. (2008). Thrombolysis with alteplase 3 to 4.5 hours after acute ischemic stroke. N Engl J Med *359*, 1317-1329.
Hahn, E. L. (1950). Spin echoes. Physical Rev *80*, 580-594.
Halle, B. (1999). Magnetic Relaxation Dispersion: Principles and Application, In Hydration Processes in Biology: Theoretical and Experimental Approaches, M.-C. Bellisent-Funel, ed. (Amsterdam: IOS Press).
Hansen, A. J., and Lauritzen, M. (1984). The role of spreading depression in acute brain disorders. An Acad Bras Cienc *56*, 457-479.
Hansen, A. J., and Zeuthen, T. (1981). Extracellular ion concentrations during spreading depression and ischemia in the rat brain cortex. Acta Physiol Scand *113*, 437-445.
Haris, M., McArdle, E., Fenty, M., Singh, A., Davatzikos, C., Trojanowski, J. Q., Melhem, E. R., Clark, C. M., and Borthakur, A. (2009). Early marker for Alzheimer's disease: hippocampus T1rho (T(1rho)) estimation. J Magn Reson Imaging *29*, 1008-1012.
Hasegawa, Y., Formato, J. E., Latour, L. L., Gutierrez, J. A., Liu, K. F., Garcia, J. H., Sotak, C. H., and Fisher, M. (1996). Severe transient hypoglycemia causes reversible change in the apparent diffusion coefficient of water. Stroke *27*, 1648-1655; discussion 1655-1646.
Hazlewood, C. F., Chang, D. C., Nichols, B. L., and Woessner, D. E. (1974). Nuclear magnetic resonance transverse relaxation times of water protons in skeletal muscle. Biophys J *14*, 583-606.
Heckl, S. (2007). Future contrast agents for molecular imaging in stroke. Curr Med Chem *14*, 1713-1728.
Heiss, W. D. (1983). Flow thresholds of functional and morphological damage of brain tissue. Stroke *14*, 329-331.
Henkelman, R. M., Huang, X., Xiang, Q.-S., Stanisz, G. J., Swanson, S. D., and Bronskill, M. J. (1993). Quantitative interpretation of magnetization transfer. Magn Reson Med *29*, 759-766.
Henkelman, R. M., Stanisz, G. J., and Graham, S. J. (2001). Magnetization transfer in MRI: a review. NMR Biomed *14*, 57-64.

Hochachka, P. W. (1999). The metabolic implications of intracellular circulation. Proc Natl Acad Sci U S A *96*, 12233-12239.
Hochachka, P. W., and Mommsen, T. P. (1983). Protons and anaerobiosis. Science *219*, 1391-1397.
Hoehn-Berlage, M., Norris, D. G., Kohno, K., Mies, G., Leibfritz, D., and Hossmann, K. A. (1995). Evolution of regional changes in apparent diffusion coefficient during focal ischemia of rat brain: the relationship of quantitative diffusion NMR imaging to reduction in cerebral blood flow and metabolic disturbances. J Cereb Blood Flow Metab *15*, 1002-1011.
Hoehn, M., Nicolay, K., Franke, C., and van der Sanden, B. (2001). Application of magnetic resonance to animal models of cerebral ischemia. J Magn Reson Imaging *14*, 491-509.
Hossmann, K. A. (1994). Viability thresholds and the penumbra of focal ischemia. Ann Neurol *36*, 557-565.
Howe, F. A., Maxwell, R. J., Saunders, D. E., Brown, M. N., and Griffiths, J. R. (1993). Proton spectroscopy in vivo. Magn Reson Quart *9*, 31-59.
Huckabee, W. E. (1958). Relationships of pyruvate and lactate during anaerobic metabolism. I. Effects of infusion of pyruvate or glucose and of hyperventilation. J Clin Invest *37*, 244-254.
Inuzuka, T., Tamura, A., Sato, S., Kirino, T., Yanagisawa, K., Toyoshima, I., and Miyatake, T. (1990). Changes in the concentrations of cerebral proteins following occlusion of the middle cerebral artery in rats. Stroke *21*, 917-922.
Jacobs, M. A., Knight, R. A., Soltanian-Zadeh, H., Zheng, Z. G., Goussev, A. V., Peck, D. J., Windham, J. P., and Chopp, M. (2000). Unsupervised segmentation of multiparameter MRI in experimental cerebral ischemia with comparison to T2, diffusion, and ADC MRI parameters and histopathological validation. J Magn Reson Imaging *11*, 425-437.
Jiang, Q., Chopp, M., Zhang, Z. G., Helpern, J. A., Ordidge, R. J., Ewing, J., Jiang, P., and Marchese, B. A. (1994). The effect of hypothermia on transient focal ischemia in rat brain evaluated by diffusion- and perfusion-weighted NMR imaging. J Cereb Blood Flow Metab *14*, 732-741.
Jiang, Q., Zhang, Z. G., Chopp, M., Helpern, J. A., Ordidge, R. J., Garcia, J. H., Marchese, B. A., Qing, Z. X., and Knight, R. A. (1993). Temporal evolution and spatial distribution of the diffusion constant of water in rat brain after trnasient middle cerebral artery occlusion. J Neurol Sci *120*, 123-130.
Jones, G. P. (1966). Spin-lattice relaxation in the rotating frame: weak-collision case. Phys Rev *148*, 332-335.
Kato, H., Kogure, K., Ohtomo, H., Izumiyama, M., Tobita, M., Matsui, S., Yamamoto, E., Kohno, H., Ikebe, Y., and Watanabe, T. (1986). Characterization of experimental ischemic brain edema utilizing proton nuclear magnetic resonance imaging. J Cereb Blood Flow Metab *6*, 212-221.
Kato, H., Kogure, K., Ohtomo, H., Tobita, M., Matsui, S., Yamamoto, E., and Kohno, H. (1985). Correlations between proton nuclear magnetic resonance imaging and retrospective histochemical images in experimental cerebral infarction. J Cereb Blood Flow Metab *5*, 267-274.
Katsura, K., Asplund, B., Ekholm, A., and Siesjö, B. K. (1992). Extra- and intracellular pH in the brain during ischaemia, related to tissue lactate content in normo- and hypercapnic rats. Eur J Neurosci *4*, 166-176.
Katsura, K., Ekholm, A., Asplund, B., and Siesjo, B. K. (1991). Extracellular pH in the brain during ischemia: relationship to the severity of lactic acidosis. J Cereb Blood Flow Metab *11*, 597-599.
Kauppinen, R. A., and Williams, S. R. (1994). Nuclear magnetic resonance spectroscopy studies of the brain. Prog Neurobiol *44*, 87-118.
Kaur, C., and Ling, E. A. (2008). Blood brain barrier in hypoxic-ischemic conditions. Curr Neurovasc Res *5*, 71-81.
Kettunen, M. I., Grohn, O. H., Penttonen, M., and Kauppinen, R. A. (2001). Cerebral T1rho relaxation time increases immediately upon global ischemia in the rat independently of blood glucose and anoxic depolarization. Magn Reson Med *46*, 565-572.
Kettunen, M. I., Gröhn, O. H. J., Lukkarinen, J. A., Vainio, P., Silvennoinen, M. J., and Kauppinen, R. A. (2000). Interrelations of T_1 and diffusion of water in acute cerebral ischemia of the rat. Magn Reson Med *44*, 833-839.
Kimelberg, H. K., Nestor, N. B., and Feustel, P. J. (2004). Inhibition of release of taurine and excitatory amino acids in ischemia and neuroprotection. Neurochem Res *29*, 267-274.
Klatzo, I. (1967). Presidental address. Neuropathological aspects of brain edema. J Neuropathol Exp Neurol *26*, 1-14.
Kleinschmidt, A., Merboldt, K. D., Hanicke, W., Steinmetz, H., and Frahm, J. (1994). Correlational imaging of thalamocortical coupling in the primary visual pathway of the human brain. J Cereb Blood Flow Metab *14*, 952-957.
Knight, R. A., Dereski, M. O., Helpern, J. A., Ordidge, R. J., and Chopp, M. (1994). Magnetic resonance imaging assessment of evolving focal cerebral ischemia. Comparison with histopathology in rats. Stroke *25*, 1252-1261.
Knispel, R. R., Thompson, R. T., and Pintar, M. M. (1974). Dispersion of proton spin-lattice relaxation in tissues. J Magn Reson *14*, 44-51.
Kochanek, P. M., Berger, R. P., Bayir, H., Wagner, A. K., Jenkins, L. W., and Clark, R. S. (2008). Biomarkers of primary and evolving damage in traumatic and ischemic brain injury: diagnosis, prognosis, probing mechanisms, and therapeutic decision making. Curr Opin Crit Care *14*, 135-141.
Koenig, S. H., and Brown III, R. D. (1994). Relaxometry and the source of contrast in MRI, In NMR in physiology and biomedicine, R. J. Gillies, ed. (San Diego, USA: Academic Press), pp. 57-73.

Kondziolka, D., Wechsler, L., Goldstein, S., Meltzer, C., Thulborn, K. R., Gebel, J., Jannetta, P., DeCesare, S., Elder, E. M., McGrogan, M., *et al.* (2000). Transplantation of cultured human neuronal cells for patients with stroke. Neurology *55*, 565-569.

Krieger, D. W., and Yenari, M. A. (2004). Therapeutic hypothermia for acute ischemic stroke: what do laboratory studies teach us? Stroke *35*, 1482-1489.

Kristian, T., and Siesjo, B. K. (1998). Calcium in ischemic cell death. Stroke *29*, 705-718.

Kumar, A., Welti, D., and Ernst, R. (1975). NMR Fourier zeugmatography. Journal of Magnetic Resonance *18*, 69-83.

Lamminen, A. E., Tanttu, J. I., Sepponen, R. E., Pihko, H., and Korhola, O. A. (1993). $T_{1\rho}$ dispersion imaging of diseased muscle tissue. Br J Radiol *66*, 783-787.

Lansberg, M. G., Thijs, V. N., O'Brien, M. W., Ali, J. O., de Crespigny, A. J., Tong, D. C., Moseley, M. E., and Albers, G. W. (2001). Evolution of apparent diffusion coefficient, diffusion-weighted, and T2-weighted signal intensity of acute stroke. AJNR Am J Neuroradiol *22*, 637-644.

Latour, L. L., Svoboda, K., Mitra, P. P., and Sotak, C. H. (1994). Time-dependent diffusion of water in a biological model system. Proc Natl Acad Sci USA *91*, 1229-1233.

Lauterbur, P. (1973). Image Formation by Induced Local Interactions: Examples Employing Nuclear Magnetic Resonance. Nature *242*, 190-191.

Le Bihan, D., Mangin, J. F., Poupon, C., Clark, C. A., Pappata, S., Molko, N., and Chabriat, H. (2001). Diffusion tensor imaging: concepts and applications. J Magn Reson Imaging *13*, 534-546.

Li, L., Jiang, Q., Ding, G., Zhang, L., Zhang, Z. G., Ewing, J. R., Knight, R. A., Kapke, A., Soltanian-Zadeh, H., and Chopp, M. (2005). Map-ISODATA demarcates regional response to combination rt-PA and 7E3 F(ab')2 treatment of embolic stroke in the rat. J Magn Reson Imaging *21*, 726-734.

Li, L., Jiang, Q., Zhang, L., Ding, G., Gang Zhang, Z., Li, Q., Ewing, J. R., Lu, M., Panda, S., Ledbetter, K. A., *et al.* (2007). Angiogenesis and improved cerebral blood flow in the ischemic boundary area detected by MRI after administration of sildenafil to rats with embolic stroke. Brain Res *1132*, 185-192.

Li, L., Jiang, Q., Zhang, L., Ding, G., Wang, L., Zhang, R., Zhang, Z. G., Li, Q., Ewing, J. R., Kapke, A., *et al.* (2006). Ischemic cerebral tissue response to subventricular zone cell transplantation measured by iterative self-organizing data analysis technique algorithm. J Cereb Blood Flow Metab *26*, 1366-1377.

Li, Y., Chopp, M., Chen, J., Wang, L., Gautam, S. C., Xu, Y. X., and Zhang, Z. (2000). Intrastriatal transplantation of bone marrow nonhematopoietic cells improves functional recovery after stroke in adult mice. J Cereb Blood Flow Metab *20*, 1311-1319.

Liepinsh, E., and Otting, G. (1996). Proton exchange rates from amino acid side chains-implications for image contrast. Magn Reson Med *35*, 30-42.

Lin, W., Venkatesan, R., Gurleyik, K., He, Y. Y., Powers, W. J., and Hsu, C. Y. (2000). An absolute measurement of brain water content using magnetic resonance imaging in two focal cerebral ischemic rat models. J Cereb Blood Flow Metab *20*, 37-44.

Longa, E. Z., Weinstein, P. R., Carlson, S., and Cummins, R. (1989). Reversible middle cerebral artery occlusion without craniectomy in rats. Stroke *20*, 84-91.

Lu, M., Mitsias, P. D., Ewing, J. R., Soltanian-Zadeh, H., Bagher-Ebadian, H., Zhao, Q., Oja-Tebbe, N., Patel, S. C., and Chopp, M. (2005). Predicting final infarct size using acute and subacute multiparametric MRI measurements in patients with ischemic stroke. J Magn Reson Imaging *21*, 495-502.

Lythgoe, M. F., Thomas, D. L., Calamante, F., Pell, G. S., King, M. D., Busza, A. L., Sotak, C. H., Williams, S. R., Ordidge, R. J., and Gadian, D. G. (2000). Acute changes in MRI diffusion, perfusion, T(1), and T(2) in a rat model of oligemia produced by partial occlusion of the middle cerebral artery. Magn Reson Med *44*, 706-712.

Macri, M. A., D'Alessandro, N., Di Giulio, C., Di Iorio, P., Di Luzio, S., Giuliani, P., Bianchi, G., and Esposito, E. (2006). Regional changes in the metabolite profile after long-term hypoxia-ischemia in brains of young and aged rats: a quantitative proton MRS study. Neurobiol Aging *27*, 98-104.

Mäkelä, H., Kettunen, M., Gröhn, O., and Kauppinen, R. (2002). Quantitative T(1rho) and magnetization transfer magnetic resonance imaging of acute cerebral ischemia in the rat. J Cereb Blood Flow Metab *22*, 547-558.

Mäkelä, H. I., Gröhn, O. H., Kettunen, M. I., and Kauppinen, R. A. (2001). Proton exchange as a relaxation mechanism for T1 in the rotating frame in native and immobilized protein solutions. Biochem Biophys Res Commun *289*, 813-818.

Markkola, A. T., Aronen, H. J., Ramadan, U. A., Halavaara, J. T., Tanttu, J. I., and Sepponen, R. E. (1998). Determination of T1rho values for head and neck tissues at 0.1 T: a comparison to T1 and T2 relaxation times. Magn Reson Imaging *16*, 377-383.

Markus, R., Reutens, D. C., Kazui, S., Read, S., Wright, P., Pearce, D. C., Tochon-Danguy, H. J., Sachinidis, J. I., and Donnan, G. A. (2004). Hypoxic tissue in ischaemic stroke: persistence and clinical consequences of spontaneous survival. Brain *127*, 1427-1436.

Martin, L. J., Al-Abdulla, N. A., Brambrink, A. M., Kirsch, J. R., Sieber, F. E., and Portera-Cailliau, C. (1998). Neurodegeneration in excitotoxicity, global cerebral ischemia, and target deprivation: A perspective on the contributions of apoptosis and necrosis. Brain Res Bull *46*, 281-309.

Martinez-Sanchez, P., Diez-Tejedor, E., Fuentes, B., Ortega-Casarrubios, M. A., and Hacke, W. (2007). Systemic reperfusion therapy in acute ischemic stroke. Cerebrovasc Dis *24 Suppl 1*, 143-152.

Meiboom, S., and Gill, D. (1958). Modified spin-echo method for measuring nuclear relaxation times. Rev Sci Instr *29*, 688-691.

Michaeli, S., Burns, T. C., Kudishevich, E., Harel, N., Hanson, T., Sorce, D. J., Garwood, M., and Low, W. C. (2009). Detection of neuronal loss using T(1rho) MRI assessment of (1)H(2)O spin dynamics in the aphakia mouse. J Neurosci Methods *177*, 160-167.

Michaeli, S., Grohn, H., Grohn, O., Sorce, D. J., Kauppinen, R., Springer, C. S., Jr., Ugurbil, K., and Garwood, M. (2005). Exchange-influenced T2rho contrast in human brain images measured with adiabatic radio frequency pulses. Magnetic Resonance in Medicine *53*, 823-829.

Michaeli, S., Sorce, D. J., Idiyatullin, D., Ugurbil, K., and Garwood, M. (2004). Transverse relaxation in the rotating frame induced by chemical exchange. J Magn Reson *169*, 293-299.

Michaeli, S., Sorce, D. J., Springer, C. S., Jr., Ugurbil, K., and Garwood, M. (2006). T1rho MRI contrast in the human brain: modulation of the longitudinal rotating frame relaxation shutter-speed during an adiabatic RF pulse. J Magn Reson *181*, 135-147.

Mies, G., Ishimaru, S., Xie, Y., Seo, K., and Hossmann, K. A. (1991). Ischemic thresholds of cerebral protein synthesis and energy state following middle cerebral artery occlusion in rat. J Cereb Blood Flow Metab *11*, 753-761.

Minematsu, K., Li, L., Sotak, C. H., Davis, M. A., and Fisher, M. (1992). Reversible focal ischemic injury demostrated by diffusion-weighted magnetic resonance imaging in rats. Stroke *23*, 1304-1311.

Mitsias, P. D., Jacobs, M. A., Hammoud, R., Pasnoor, M., Santhakumar, S., Papamitsakis, N. I., Soltanian-Zadeh, H., Lu, M., Chopp, M., and Patel, S. C. (2002). Multiparametric MRI ISODATA ischemic lesion analysis: correlation with the clinical neurological deficit and single-parameter MRI techniques. Stroke *33*, 2839-2844.

Miyabe, M., Mori, S., van Zijl, P. C. M., Kirsch, J. R., Eleff, S. M., Koehler, R. C., and Traystman, R. J. (1996). Correlation of the average water diffusion constant with cerebral blood flow and ischemic damage after transient middle cerebral artery occlusion in cats. J Cereb Blood Flow Metab *16*, 881-891.

Modo, M., Roberts, T. J., Sandhu, J. K., and Williams, S. C. (2004). In vivo monitoring of cellular transplants by magnetic resonance imaging and positron emission tomography. Expert Opin Biol Ther *4*, 145-155.

Moonen, C. T. W., van Zijl, P. C. M., Frank, J. A., Le Bihan, D., and Becker, E. D. (1990). Functional magnetic resonance imaging in medicine and physiology. Science *250*, 53-60.

Mori, S., Crain, B. J., Chacko, V. P., and van Zijl, P. C. (1999). Three-dimensional tracking of axonal projections in the brain by magnetic resonance imaging. Ann Neurol *45*, 265-269.

Mori, S., Eleff, S. M., Pilatus, U., Mori, N., and van Zijl, P. C. (1998). Proton NMR spectroscopy of solvent-saturable resonances: a new approach to study pH effects in situ. Magn Reson Med *40*, 36-42.

Mori, S., and van Zijl, P. C. M. (1995). Diffusion weighting by the trace of the diffusion tensor within a single scan. Magn Reson Med *33*, 41-52.

Moseley, M. E., Cohen, Y., Mintorovitch, J., Chileuitt, L., Shimizu, H., Kucharczyk, J., Wendland, M. F., and Weinstein, P. R. (1990). Early detection of regional cerebral ischemia in cats: comparison of diffusion- and T_2-weighted MRI and spectroscopy. Magn Reson Med *14*, 330-346.

Murray, C. J., and Lopez, A. D. (1997). Mortality by cause for eight regions of the world: Global Burden of Disease Study. Lancet *349*, 1269-1276.

Naruse, S., Horikawa, Y., Tanaka, C., Hirakawa, K., Nishikawa, H., and Yoshizaki, K. (1986). Significance of proton relaxation time measurement in brain edema, cerebral infarction and brain tumors. Magn Reson Imaging *4*, 293-304.

Närväinen, J., Hubbard, P. L., Kauppinen, R. A., and Morris, G. A. (2009). Z-spectroscopy with alternating phase irradiation - ZAPI. submitted.

Niizuma, K., Endo, H., and Chan, P. H. (2009). Oxidative stress and mitochondrial dysfunction as determinants of ischemic neuronal death and survival. J Neurochem *109 Suppl 1*, 133-138.

Nitatori, T., Sato, N., Waguri, S., Karasawa, Y., Araki, H., Shibanai, K., Kominami, E., and Uchiyama, Y. (1995). Delayed neuronal death in the CA1 pyramidal cell layer of the gerbil hippocampus following transient ischemia is apoptosis. J Neurosci *15*, 1001-1011.

Ogawa, S., Lee, T. M., Kay, A. R., and Tank, D. W. (1990). Brain magnetic resonance imaging with contrast dependent on blood oxygenation. Proc Natl Acad Sci USA *87*, 9868-9872.

Okada, Y., Shimizu, T., Maeno, E., Tanabe, S., Wang, X., and Takahashi, N. (2006). Volume-sensitive chloride channels involved in apoptotic volume decrease and cell death. J Membr Biol *209*, 21-29.

Ordidge, R. J., Helpern, J. A., Knight, R. A., Qing, Z., and Welch, K. M. A. (1991). Investigation of cerebral ischemia using magnetization transfer contrast (MTC) MR imaging. Magn Reson Imaging *9*, 895-902.

Parsons, M. W., Yang, Q., Barber, P. A., Darby, D. G., Desmond, P. M., Gerraty, R. P., Tress, B. M., and Davis, S. M. (2001). Perfusion magnetic resonance imaging maps in hyperacute stroke: relative cerebral blood flow most accurately identifies tissue destined to infarct. Stroke *32*, 1581-1587.

Paxinos, G. T., and Watson, C. (1996). The Rat Brain in Stereotaxic Coordinates. (London: Academic Press).

Pekar, J., Jezzard, P., Roberts, D. A., Leigh, J. S., Jr., Frank, J. A., and McLaughlin, A. C. (1996). Perfusion imaging with compensation for asymmetric magnetization transfer effects. Magn Reson Med *35*, 70-79.

Pierpaoli, C., Righini, A., Linfante, I., Tao-Cheng, J. H., Alger, J. R., and Di Chiro, G. (1993). Histopathologic correlates of abnormal water diffusion in cerebral ischemia: diffusion-weigthed MR imaging and ligth and electron microscopic study. Radiology *189*, 439-448.

Pignataro, G., Scorziello, A., Di Renzo, G., and Annunziato, L. (2009). Post-ischemic brain damage: effect of ischemic preconditioning and postconditioning and identification of potential candidates for stroke therapy. Febs J *276*, 46-57.

Popel, A. S., and Gross, J. F. (1979). Analysis of oxygen diffusion from arteriolar networks. Am J Physiol *237*, 681-689.

Powers, W. J., Grubb, R. L., Jr., Darriet, D., and Raichle, M. E. (1985). Cerebral blood flow and cerebral metabolic rate of oxygen requirements for cerebral function and viability in humans. J Cereb Blood Flow Metab *5*, 600-608.

Powers, W. J., Press, G. A., Grubb, R. L., Jr., Gado, M., and Raichle, M. E. (1987). The effect of hemodynamically significant carotid artery disease on the hemodynamic status of the cerebral circulation. Ann Intern Med *106*, 27-34.

Purcell, E. M., Torrey, H. C., and Pound, R. V. (1946). Resonance absorption by nuclear magnetic moments in a solid. Phys Rev *69*, 37-38.

Quirk, J. D., Bretthorst, G. L., Duong, T. Q., Snyder, A. Z., Springer, C. S., Jr., Ackerman, J. J., and Neil, J. J. (2003). Equilibrium water exchange between the intra- and extracellular spaces of mammalian brain. Magn Reson Med *50*, 493-499.

Rabi, I. I., Millman, S., Kusch, P., and Zacharias, J. R. (1938). A new method for measuring nuclear magnetic moment. Phys Rev *53*, 318.

Ramadan, U. A., Markkola, A. T., Halavaara, J., Tanttu, J., Hakkinen, A. M., and Aronen, H. J. (1998). On- and off-resonance spin-lock MR imaging of normal human brain at 0.1 T: possibilities to modify image contrast. Magn Reson Imaging *16*, 1191-1199.

Regatte, R. R., Akella, S. V., Borthakur, A., Kneeland, J. B., and Reddy, R. (2003). In vivo proton MR three-dimensional T1rho mapping of human articular cartilage: initial experience. Radiology *229*, 269-274.

Reith, J., Jorgensen, H. S., Pedersen, P. M., Nakayama, H., Raaschou, H. O., Jeppesen, L. L., and Olsen, T. S. (1996). Body temperature in acute stroke: relation to stroke severity, infarct size, mortality, and outcome. Lancet *347*, 422-425.

Reith, W., Hasegawa, Y., Latour, L. L., Dardzinski, B. J., Sotak, C. H., and Fisher, M. (1995). Multislice diffusion mapping for 3-D evolution of cerebral ischemia in a rat stroke model. Neurology *45*, 172-177.

Rivers, C. S., Wardlaw, J. M., Armitage, P. A., Bastin, M. E., Carpenter, T. K., Cvoro, V., Hand, P. J., and Dennis, M. S. (2006). Do acute diffusion- and perfusion-weighted MRI lesions identify final infarct volume in ischemic stroke? Stroke *37*, 98-104.

Rohl, L., Ostergaard, L., Simonsen, C. Z., Vestergaard-Poulsen, P., Andersen, G., Sakoh, M., Le Bihan, D., and Gyldensted, C. (2001). Viability thresholds of ischemic penumbra of hyperacute stroke defined by perfusion-weighted MRI and apparent diffusion coefficient. Stroke *32*, 1140-1146.

Rordorf, G., Koroshetz, W. J., Copen, W. A., Cramer, S. C., Schaefer, P. W., Budzik, R. F., Jr., Schwamm, L. H., Buonanno, F., Sorensen, A. G., and Gonzalez, G. (1998). Regional ischemia and ischemic injury in patients with acute middle cerebral artery stroke as defined by early diffusion-weighted and perfusion-weighted MRI. Stroke *29*, 939-943.

Rosen, B. R., Belliveau, J. W., Vevea, J. M., and Brady, T. J. (1990). Perfusion imaging with NMR contrast agents. Magn Reson Med *14*, 249-265.

Rossi, D. J., Brady, J. D., and Mohr, C. (2007). Astrocyte metabolism and signaling during brain ischemia. Nat Neurosci *10*, 1377-1386.

Roussel, S. A., van Bruggen, N., King, M. D., and Gadian, D. G. (1995). Identification of collaterally perfused areas following focal ischemia in the rat by comparison of gradient echo and diffusion-weighted MRI. J Cereb Blood Flow Metab *15*, 578-586.

Roussel, S. A., Vanbruggen, N., King, M. D., Houseman, J., Williams, S. R., and Gadian, D. G. (1994). Monitoring the initial expansion of focal ischaemic changes by diffusion-weighted MRI using a remote controlled method of occlusion. NMR Biomed *7*, 21-28.

Santyr, G. E., Fairbanks, E. J., Kelcz, F., and Sorenson, J. A. (1994). Off-resonance spin locking for MR imaging. Magn Reson Med *32*, 43-51.

Santyr, G. E., Henkelman, R. M., and Bronskill, M. J. (1988). Variation in measured transverse relaxation in tissue resulting from spin locking with rhe CPMG sequence. J Magn Reson *79*, 28-44.

Santyr, G. E., Henkelman, R. M., and Bronskill, M. J. (1989). Spin locking for magnetic resoance imaging with application to human breast. Magn Reson Med *12*, 25-37.

Schomer, D. F., Marks, M. P., Steinberg, G. K., Johnstone, I. M., Boothroyd, D. B., Ross, M. R., Pelc, N. J., and Enzmann, D. R. (1994). The anatomy of the posterior communicating artery as a risk factor for ischemic cerebral infarction. N Engl J Med *330*, 1565-1570.

Schumann, P., Touzani, O., Young, A. R., Morello, R., Baron, J. C., and MacKenzie, E. T. (1998). Evaluation of the ratio of cerebral blood flow to cerebral blood volume as an index of local cerebral perfusion pressure. Brain *121*, 1369-1379.

Schurr, A. (2002). Lactate, glucose and energy metabolism in the ischemic brain (Review). Int J Mol Med *10*, 131-136.

Schwab, S., Schwarz, S., Spranger, M., Keller, E., Bertram, M., and Hacke, W. (1998). Moderate hypothermia in the treatment of patients with severe middle cerebral artery infarction. Stroke *29*, 2461-2466.

Sepponen, R., Tanttu, J. I., Suramo, I., Sipponen, J. I., and Kaste, M. (1986). $T_{1\rho}$ and $T_{1\rho}$ dispersion imaging in patients with cerebral infarction., Paper presented at: 5th Annual Meeting of Society of Magnetic Resonance in Medicine (Montreal, Canada).

Sepponen, R. E., Pohjonen, J. A., Sipponen, J. T., and Tanttu, J. I. (1985). A method for $T_{1\rho}$ imaging. J Comput Assist Tomogr *9*, 1007-1011.

Shen, Q., Ren, H., Fisher, M., Bouley, J., and Duong, T. Q. (2004). Dynamic tracking of acute ischemic tissue fates using improved unsupervised ISODATA analysis of high-resolution quantitative perfusion and diffusion data. J Cereb Blood Flow Metab *24*, 887-897.

Shen, Q., Ren, H., Fisher, M., and Duong, T. Q. (2005). Statistical prediction of tissue fate in acute ischemic brain injury. J Cereb Blood Flow Metab *25*, 1336-1345.

Sierra, A., Michaeli, S., Niskanen, J.-P., Valonen, P. K., Gröhn, H. I., Ylä-Herttuala, S., Garwood, M., and Gröhn, O. H. (2008). Water spin dynamics during apoptotic cell death in glioma gene therapy probed by T1rho and T2rho. Magn Reson Med.

Siesjö, B. K. (1992). Pathophysiology and treatment of focal cerebral ischemia. Part I: Pathophysiology. J Neurosurg *77*, 169-184.

Siesjö, B. K., Ekholm, A., Katsura, K., and Theander, S. (1990). Acid-base changes during complete brain ischemia. Stroke *21*, III194-199.

Siesjö, B. K., and Nilsson, L. (1971). The influence of arterial hypoxemia upon labile phosphates and upon extracellular and intracellular lactate and pyruvate concentrations in the rat brain. Scand J Clin Lab Invest *27*, 83-96.

Silver, M. S., Joseph, R. I., and Hoult, D. I. (1984). Highly selective $\pi/2$ and π pulse generation. J Magn Reson *59*, 347-351.

Sims, N. R., and Zaidan, E. (1995). Biochemical changes associated with selective neuronal death following short-term cerebral ischaemia. International Journal of Biochemistry & Cell Biology *27*, 531-550.

Slemmer, J. E., Shacka, J. J., Sweeney, M. I., and Weber, J. T. (2008). Antioxidants and free radical scavengers for the treatment of stroke, traumatic brain injury and aging. Curr Med Chem *15*, 404-414.

Smith, M.-L., von Hanwehr, R., and Siesjö, B. K. (1986). Changes in extra- and intracellular pH in the brain during and following ischemia in hyperglycemic and in moderately hypolycemic rats. J Cereb Blood Flow Metabol *6*, 574 - 583.

Sobesky, J., Zaro Weber, O., Lehnhardt, F. G., Hesselmann, V., Neveling, M., Jacobs, A., and Heiss, W. D. (2005). Does the mismatch match the penumbra? Magnetic resonance imaging and positron emission tomography in early ischemic stroke. Stroke *36*, 980-985.

Sokoloff, L. (1989). Circulation and Energy Metabolism of the Brain, In Basic Neurochemistry, G. Siegel, B. Arganoff, R. W. Albers, and P. Molinoff, eds. (New York: Raven Press), pp. 565-590.

Solomon, I. (1959). Rotary Spin Echoes. Phys Rev Lett *2*, 301-302.

Soltanian-Zadeh, H., Pasnoor, M., Hammoud, R., Jacobs, M. A., Patel, S. C., Mitsias, P. D., Knight, R. A., Zheng, Z. G., Lu, M., and Chopp, M. (2003). MRI tissue characterization of experimental cerebral ischemia in rat. J Magn Reson Imaging *17*, 398-409.

Sorensen, A. G., Buonanno, F. S., Gonzalez, R. G., Schwamm, L. H., Lev, M. H., Huang-Hellinger, F. R., Reese, T. G., Weisskoff, R. M., Davis, T. L., Suwanwela, N., *et al.* (1996). Hyperacute stroke: evaluation with combined multisection diffusion-weighted and hemodynamic weighted echo-planar imaging. Radiology *199*, 391-401.

Sotak, C. H. (2002). The role of diffusion tensor imaging in the evaluation of ischemic brain injury - a review. NMR Biomed *15*, 561-569.

Stejskal, E. O., and Tanner, J. E. (1965). Spin diffusion measurements: spin-echoes in the presence of a time-dependent field gradient. JChem Phys *42*, 288-292.

Strong, K., Mathers, C., and Bonita, R. (2007). Preventing stroke: saving lives around the world. Lancet Neurol *6*, 182-187.

Sun, P. Z., Zhou, J., Huang, J., and van Zijl, P. (2007a). Simplified quantitative description of amide proton transfer (APT) imaging during acute ischemia. Magn Reson Med *57*, 405-410.

Sun, P. Z., Zhou, J., Sun, W., Huang, J., and van Zijl, P. C. (2007b). Detection of the ischemic penumbra using pH-weighted MRI. J Cereb Blood Flow Metab *27*, 1129-1136.

Swanson, R. A., Chen, J., and Graham, S. H. (1994). Glucose can fuel glutamate uptake in ischemic brain. J Cereb Blood Flow Metab *14*, 1-6.
Swanson, R. A., Farrell, K., and Stein, B. A. (1997). Astrocyte energetics, function, and death under conditions of incomplete ischemia: a mechanism of glial death in the penumbra. Glia *21*, 142-153.
Szafer, A., Zhong, J., and Gore, J. C. (1995). Theoretical model for water diffusion in tissues. Magn Reson Med *33*, 697-712.
Takano, K., Latour, L. L., Formato, J. E., Carano, R. A., Helmer, K. G., Hasegawa, Y., Sotak, C. H., and Fisher, M. (1996). The role of spreading depression in focal ischemia evaluated by diffusion mapping. Ann Neurol *39*, 308-318.
Takano, T., Oberheim, N., Cotrina, M. L., and Nedergaard, M. (2009). Astrocytes and ischemic injury. Stroke *40*, S8-12.
Taylor, T. N., Davis, P. H., Torner, J. C., Holmes, J., Meyer, J. W., and Jacobson, M. F. (1996). Lifetime cost of stroke in the United States. Stroke *27*, 1459-1466.
Thomas, D. L., Lythgoe, M. F., Pell, G. S., Calamante, F., and Ordidge, R. J. (2000). The measurement of diffusion and perfusion in biological systems using magnetic resonance imaging. Phys Med Biol *45*, R97-138.
Tortosa, A., Rivera, R., and Ferrer, I. (1994). Dose-related effects of cycloheximide on delayed neuronal death in the gerbil hippocampus after bilateral transitory forebrain ischemia. J Neurol Sci *121*, 10-17.
Trendelenburg, G., and Dirnagl, U. (2005). Neuroprotective role of astrocytes in cerebral ischemia: focus on ischemic preconditioning. Glia *50*, 307-320.
Tsukada, T., Watanabe, M., and Yamashima, T. (2001). Implications of CAD and DNase II in ischemic neuronal necrosis specific for the primate hippocampus. J Neurochem *79*, 1196-1206.
Ulmer, J. L., Mathews, V. P., Hamilton, C. A., Elster, A. D., and Moran, P. R. (1996). Magnetization transfer or spin-lock? An investigation of off-resonance saturation pulse imaging with varying frequency offsets. AJNR Am J Neuroradiol *17*, 805-819.
van Bruggen, N., Roberts, T. P. L., and Cremer, J. E. (1994). The application of magnetic resonance imaging to the study of experimental cerebral ischaemia. Cerebrovasc Brain Metab Rev *6*, 180-210.
van der Toorn, A., Sykova, E., Dijkhuizen, R. M., Vorisek, I., Vargova, L., Skobisova, E., van Lookeren Campagne, M., Reese, T., and Nicolay, K. (1996). Dynamic changes in water ADC, energy metabolism, extracellular space volume, and tortuosity in neonatal rat brain during global ischemia. Magn Reson Med *36*, 52-60.
van der Toorn, A., Verheul, H. B., van der Sprenkel, J. W., Tulleken, C. A., and Nicolay, K. (1994). Changes in metabolites and tissue water status after focal ischemia in cat brain assessed with localized proton MR spectroscopy. Magn Reson Med *32*, 685-691.
van Gelderen, P., de Vleeschouwer, M. H., DesPres, D., Pekar, J., van Zijl, P. C., and Moonen, C. T. (1994). Water diffusion and acute stroke. Magn Reson Med *31*, 154-163.
van Zijl, P. C., Zhou, J., Mori, N., Payen, J. F., Wilson, D., and Mori, S. (2003). Mechanism of magnetization transfer during on-resonance water saturation. A new approach to detect mobile proteins, peptides, and lipids. Magn Reson Med *49*, 440-449.
Verhaegen, M. J., Todd, M. M., Hindman, B. J., and Warner, D. S. (1993). Cerebral autoregulation during moderate hypothermia in rats. Stroke *24*, 407-414.
Verheul, H. B., Balazs, R., Berkelbach van der Sprenkel, J. W., Tulleken, C. A., Nicolay, K., Tamminga, K. S., and van Lookeren Campagne, M. (1994). Comparison of diffusion-weighted MRI with changes in cell volume in a rat model of brain injury. NMR Biomed *7*, 96-100.
Verheul, H. B., Berkelbach van der Sprenkel, J. W., Tulleken, C. A., Tamminga, K. S., and Nicolay, K. (1992). Temporal evolution of focal cerebral ischemia in the rat assessed by T2-weighted and diffusion-weighted magnetic resonance imaging. Brain Topogr *5*, 171-176.
Villringer, A., Rosen, B. R., Belliveau, J. W., Ackerman, J. L., Lauffer, R. B., Buxton, R. B., Chao, Y. S., Wedeen, V. J., and Brady, T. J. (1988). Dynamic imaging with lanthanide chelates in normal brain: contrast due to magnetic susceptibility effects. Magn Reson Med *6*, 164-174.
Virta, A., Komu, M., and Kormano, M. (1997). T1ρ of protein solutions at very low fields: dependence on molecular weight, concentration, and structure. Magn Reson Med *37*, 53-57.
Virta, A., Komu, M., Lundbom, N., and Kormano, M. (1998). T1 rho MR imaging characteristics of human anterior tibial and gastrocnemius muscles. Acad Radiol *5*, 104-110.
Warach, S., Chien, D., Li, W., Ronthal, M., and Edelman, R. R. (1992). Fast magnetic resonance diffusion-weighted imaging of acute human stroke. Neurology *42*, 1717-1723.
Warach, S., Mosley, M., Sorensen, A. G., and Koroshetz, W. S. O. (1996). Time course of diffusion imaging abnormalities in human stroke. Stroke *27*, 1254-1256.
Welch, K. M., Levine, S. R., Martin, G., Ordidge, R., van de Linde, A. M., and Halpern, J. A. (1992). Magnetic resonance spectroscopy in cerebral ischemia. Neurol Clin *10*, 1-29.

Welch, K. M., Windham, J., Knight, R. A., Nagesh, V., Hugg, J. W., Jacobs, M., Peck, D., Booker, P., Dereski, M. O., and Levine, S. R. (1995). A model to predict the histopathology of human stroke using diffusion and T2-weighted magnetic resonance imaging. Stroke *26*, 1983-1989.

Wheatley, D. N. (1985). Mini-review. On the possible importance of an intracellular circulation. Life Sci *36*, 299-307.

Wheaton, A. J., Borthakur, A., Corbo, M., Charagundla, S. R., and Reddy, R. (2004). Method for reduced SAR T1rho-weighted MRI. Magn Reson Med *51*, 1096-1102.

White, R. P., and Markus, H. S. (1997). Impaired dynamic cerebral autoregulation in carotid artery stenosis. Stroke *28*, 1340-1344.

Wick, M., Nagatomo, Y., Prielmeier, F., and Frahm, J. (1995). Alteration of intracellular metabolite diffusion in rat brain in vivo during ischemia and reperfusion. Stroke *26*, 1930-1933.

Williams, D. S., Detre, J. A., Leigh, J. S., and Koretsky, A. P. (1992). Magnetic resonance imaging of perfusion using spin inversion of arterial water. Proc Natl Acad Sci U S A *89*, 212-216.

Williams, S. R., Crockard, H. A., and Gadian, D. G. (1989). Cerebral ischaemia studied by nuclear magnetic resonance spectroscopy. Cerebrovasc Brain Metab Rev *1*, 91—114.

Wintermark, M., Albers, G. W., Alexandrov, A. V., Alger, J. R., Bammer, R., Baron, J. C., Davis, S., Demaerschalk, B. M., Derdeyn, C. P., Donnan, G. A., *et al.* (2008). Acute stroke imaging research roadmap. Stroke *39*, 1621-1628.

Wolff, S. D., and Balaban, R. S. (1989). Magnetization transfer contrast (MTC) and tissue water proton relaxation *in vivo*. Magn Reson Med *10*, 135-144.

Wong, E. C. (2005). Quantifying CBF with pulsed ASL: technical and pulse sequence factors. J Magn Reson Imaging *22*, 727-731.

Wong, E. C., Buxton, R. B., and Frank, L. R. (1998). Quantitative imaging of perfusion using a single subtraction (QUIPSS and QUIPSS II). Magn Reson Med *39*, 702-708.

Wong, E. C., Cox, R. W., and Song, A. W. (1995). Optimized Isotropic Diffusion Weighting. MRM *34*, 139-143.

Wu, O., Koroshetz, W. J., Ostergaard, L., Buonanno, F. S., Copen, W. A., Gonzalez, R. G., Rordorf, G., Rosen, B. R., Schwamm, L. H., Weisskoff, R. M., and Sorensen, A. G. (2001). Predicting tissue outcome in acute human cerebral ischemia using combined diffusion- and perfusion-weighted MR imaging. Stroke *32*, 933-942.

Wu, O., Sumii, T., Asahi, M., Sasamata, M., Ostergaard, L., Rosen, B. R., Lo, E. H., and Dijkhuizen, R. M. (2007). Infarct prediction and treatment assessment with MRI-based algorithms in experimental stroke models. J Cereb Blood Flow Metab *27*, 196-204.

Yamauchi, H., Fukuyama, H., Nagahama, Y., Nabatame, H., Nakamura, K., Yamamoto, Y., Yonekura, Y., Konishi, J., and Kimura, J. (1996). Evidence of misery perfusion and risk for recurrent stroke in major cerebral arterial occlusive diseases from PET. J Neurol Neurosurg Psychiatry *61*, 18-25.

Yongbi, M. N., Branch, C. A., and Helpern, J. A. (1998). Perfusion imaging using FOCI RF pulses. Magn Reson Med *40*, 938-943.

Zaharchuk, G., Mandeville, J. B., Bogdanov, A. A., Jr., Weissleder, R., Rosen, B. R., and Marota, J. J. (1999). Cerebrovascular dynamics of autoregulation and hypoperfusion. An MRI study of CBF and changes in total and microvascular cerebral blood volume during hemorrhagic hypotension. Stroke *30*, 2197-2204; discussion 2204-2195.

Zhou, J., Lal, B., Wilson, D., Laterra, J., and van Zilj, P. (2003a). Amide proton transfer (APT) contrast for imaging of brain tumors. Magn Reson Med *50*, 1120-1126.

Zhou, J., Payen, J., Wilson, D., Traystman, R., and van Zijl, P. (2003b). Using the amide proton signals of intracellular proteins and peptides to detect pH effects in MRI. Nat Med *9*, 1085-1090.

Zivin, J. A., Lyden, P. D., DeGirolami, U., Kochhar, A., Mazzarella, V., Hemenway, C. C., and Johnston, P. (1988). Tissue plasminogen activator. Reduction of neurologic damage after experimental embolic stroke. Arch Neurol *45*, 387-391.

Kuopio University Publications G. - A.I.Virtanen Institute

G 57. Gurevicius, Kestutis. EEG and evoked potentials as indicators of interneuron pathology in mouse models of neurological diseases.
2007. 76 p. Acad. Diss.

G 58. Leppänen, Pia. Mouse models of atherosclerosis, vascular endothelial growth factors and gene therapy.
2007. 91 p. Acad. Diss.

G 59. Keinänen, Riitta et al. The second annual post-graduate symposium of the graduate school of molecular medicine: winter school 2008.
2008. 57 p. Abstracts.

G 60. Koponen, Jonna. Lentiviral vector for gene transfer: a versatile tool for regulated gene expression, gene silencing and progenitor cell therapies.
2008. 71 p. Acad. Diss.

G 61. Ahtoniemi, Toni. Mutant Cu,Zn superoxide dismutase in amyotrophic lateral sclerosis: molecular mechanisms of neurotoxicity.
2008. 107 p. Acad. Diss.

G 62. Purhonen, Anna-Kaisa. Signals arising from the gastointestinal tract that affect food intake.
2008. 86 p. Acad. Diss.

G 63. Kaikkonen, Minna. Engineering baculo- and lentiviral vectors for enhanced and targeted gene delivery.
2008. 109 p. Acad. Diss.

G 64. Gureviciene, Irina. Changes in hippocampal synaptic plasticity in animal models of age-related memory impairment. 2
2008. 106 p. Acad. Diss.

G 65. Oikari, Sanna. Evaluation of phenotypic changes of Acyl-CoA binding protein / diazepam binding inhibitor overexpression in transgenic mice and rats.
2008. 79 p. Acad. Diss.

G 66. Laurema, Anniina. Adenoviral gene therapy and fertility: distribution studies in reproductive organs and risk of vertical transmission in female rabbits and rats.
2008. 79 p. Acad. Diss.

G 67. Immonen, Riikka. Magnetic resonance imaging of progressive changes in traumatic brain injury and epileptogenesis.
2008. 80 p. Acad. Diss.

G 69. Kinnunen, Kati. Vascular endothelial growth factors in eye diseases: pathophysiology and new therapeutic strategies for retinal and choroideal angiogenesis.
2009. 100 p. Acad. Diss.

G 70. Korpisalo-Pirinen, Petra. Angiogenic gene therapy: vascular endothelial growth factors and platedet derived growth factros in vascular growth and stabilization.
2009. 100 p. Acad. Diss.

G 71. Ketola, Anna. Gene and virotherapy against osteosarcoma.
2009. 130 p. Acad. Diss.

G 72. Heinonen, Miika. Apelin, orexin A and ghrelin levels in obesity and the metabolic syndrome.
2009. 83 p. Acad. Diss.

G 73. Lesch, Hanna. Lentiviral vectors for gene therapy: targeting, imaging and lentivirus production.
2009. 99 p. Acad. Diss.